CR-120960

COMPARISON OF AEROGRIDS AND PUNCHED PLATES FOR SMOOTHING FLOW FROM SHORT ANNULAR DIFFUSERS

By

R. L. RUMPF And W. B. SHIPPEN

The Johns Hopkins University
Applied Physics Laboratory
Silver Spring, Maryland

Prepared For

NATIONAL AERONAUTICS AND SPACE ADMINISTRATION

NASA Lewis Research Center
Contract C-54545-B
A. J. Juhasz, Project Manager

1. Report No.	2. Government Accession No.	3. Recipient's Catalog No.
CR-120960		

4. Title and Subtitle	5. Report Date
Comparison of Aerogrids and Punched Plates for Smoothing Flow from Short Annular Diffusers	July 27, 1972
	6. Performing Organization Code

7. Author(s)	8. Performing Organization Report No.
R. L. Rumpf and W. B. Shippen	
	10. Work Unit No.

9. Performing Organization Name and Address	11. Contract or Grant No.
The John Hopkins University Applied Physics Laboratory 8621 Georgia Avenue Silver Spring, Maryland 20910	NASA C-54545-B
	13. Type of Report and Period Covered
12. Sponsoring Agency Name and Address	Contractor Report
	14. Sponsoring Agency Code
National Aeronautics and Space Administration	

15. Supplementary Notes

Project Manager, Albert J. Juhasz
Airbreathing Engines Division, NASA Lewis Research Center
Cleveland, Ohio

16. Abstract

Scale model tests were conducted to evaluate the effectiveness of aerogrids and punched plates in producing flat velocity profiles downstream of short diffusers as would be used between the compressor and combustor of advanced aircraft engines.

The diffuser had an area ratio of 4.17 and a length-to-inlet-height ratio of 2.07. The aerogrids tested were plates containing 1123 contoured venturis in parallel with geometric blockages of 83, 74, and 61 percent, respectively. The punched plates contained 1123 sharp-edged orifices with blockages of 58 and 30 percent.

The results show that aerogrids, with higher effective blockage for the same pressure loss, are more effective flow-smoothing devices than the punched plates. Also, the overall pressure loss decreases and the exit velocity profile becomes flatter as either type of grid is moved closer to the diffuser exit plane.

17. Key Words (Suggested by Author(s))	18. Distribution Statement
Aerodynamic Grids Diffuser design Velocity profile control	Unclassified - unlimited

19. Security Classif. (of this report)	20. Security Classif. (of this page)	21. No. of Pages	22. Price*
Unclassified	Unclassified		

* For sale by the National Technical Information Service, Springfield, Virginia 22151

THE JOHNS HOPKINS UNIVERSITY
APPLIED PHYSICS LABORATORY
SILVER SPRING, MARYLAND

FOREWARD

The research described herein, which was conducted by The Johns Hopkins University, Applied Physics Laboratory, was performed under NASA Contract C-54545-B. The Project Manager was Mr. Albert J. Juhasz of the Airbreathing Engines Division, NASA-Lewis Research Center.

TABLE OF CONTENTS

THE JOHNS HOPKINS UNIVERSITY
APPLIED PHYSICS LABORATORY
SILVER SPRING, MARYLAND

ABSTRACT

Scale model tests were conducted to evaluate the effectiveness of aerogrids and punched plates in producing flat velocity profiles downstream of short diffusers as would be used between the compressor and combustor of advanced aircraft engines.

The diffuser had an area ratio of 4.17 and a length-to-inlet-height ratio of 2.07. The aerogrids tested were plates containing 1123 contoured venturis in parallel with geometric blockages of 83, 74, and 61 percent, respectively. The punched plates contained 1123 sharp-edged orifices with blockages of 58 and 30 percent.

The results show that aerogrids, with higher effective blockage for the same pressure loss, are more effective flow-smoothing devices than the punched plates. Also, the overall pressure loss decreases and the exit velocity profile becomes flatter as either type of grid is moved closer to the diffuser exit plane.

THE JOHNS HOPKINS UNIVERSITY
APPLIED PHYSICS LABORATORY
SILVER SPRING, MARYLAND

SUMMARY

Tests of 1/3-linear-scale models were conducted to evaluate the effectiveness of aerogrids and punched plates in producing stable, relatively flat velocity profiles downstream of a very short diffuser located between the compressor and the annular combustor of a large turbofan engine for supersonic aircraft. The aerogrids tested were plates containing 1123 contoured venturis in parallel. The punched plates contained 1123 sharp-edged orifices sized to give the same total pressure losses as corresponding aerogrids. The objective was to produce acceptable exit flow profiles while holding the overall length (full-scale) and overall total-pressure loss for the diffuser plus the grid to 6 inches (15.2 cm) and 3 percent at an inlet Mach number of 0.3, respectively. The test variables were diffuser entrance Mach number and Reynolds number (to bracket the aircraft cruise condition and the most severe engine relight condition at altitude), grid blockage (percent of diffuser exit area), grid spacing from the diffuser exit plane, and simulated circumferential and radial flow distortions at the diffuser entrance.

The diffuser tested had an area ratio of 4.17, a length-to-inlet-height ratio of 2.07, and a constant-pressure-gradient, diverging contour of 3-inch (7.62-cm) length followed by a 1-inch (2.54-cm) length of constant-angle expansion to the full annular area of the combustor. The three aerogrids tested had geometric blockage of 83, 74, and 61 percent. The two punched plates tested had geometric blockages of 58 and 30 percent and were designed to have the same total pressure losses as the first two aerogrids (83 and 74 percent blockage, respectively) at a diffuser inlet Mach number of 0.3.

The results show that the aerogrids, with higher effective blockage for the same pressure loss, are more efficient flow-smoothing devices than the punched plates. The overall pressure loss of diffuser plus grid decreases, and the exit velocity profile becomes flatter as either type of grid is moved closer to the diffuser exit plane. Only the aerogrid of 83 percent blockage effectively smoothed the circumferential distortion created at the diffuser inlet by a 64 percent solid, 10 degree sector screen. However, the aerogrid of 74 percent blockage effectively smoothed the radial (hub- and tip-peaked) inlet flow distortions with a total pressure loss of 3 percent at an inlet Mach number of 0.3.

INTRODUCTION

The experimental work described in this report was sponsored by the Airbreathing Engines Division of the NASA Lewis Research Center where research is being conducted on a full-scale turbojet diffuser and combustor. The objective of this NASA effort is to develop a diffuser-combustor combination with minimum length; a stable, reasonably flat combustor entrance velocity profile; minimum pressure loss; high combustion efficiency; and an optimum combustor exit temperature profile for maximum turbine performance.

A portion of this effort has been concentrated on the development of the diffuser alone, and NASA/LeRC and its contractors have investigated a variety of approaches to diffuser design utilizing the inlet and outlet dimensions dictated by the overall engine design (references 1-16).

In a turbojet with an axial compressor, the diffuser designer is faced with an entrance flow that is highly turbulent, with a minimum boundary layer and strong radial and circumferential velocity gradients that are unsteady in nature. Similar diffuser entrance conditions have been encountered with ramjet engine combustion chambers used in supersonic guided missiles. One device that has been used successfully to prevent flow separation in a minimum-length diffuser section in ramjets is an "aerodynamic grid," which is a plate containing hundreds of small venturis in parallel, arranged as close together as practical in a hexagonal pattern. Such a device, located between the diffuser and the combustor, was first used on the engines for the Bomarc missile, and a patent was issued to the Boeing Company (reference 16). This technique has since been applied to the engines for the Triton and Long Range Typhon missiles developed by the Applied Physics Laboratory of The Johns Hopkins University and to several APL/JHU exploratory and advanced development propulsion programs. The basic objective of the work reported here was to apply this design knowledge on aerodynamic grids to the design of annular turbojet diffusers of minimum length.

Many other approaches for shortening diffusers have been investigated in the past. The general problem is that the diffuser performance decreases as the angle of divergence increases, and unacceptably high pressure losses and regions of flow separation have often resulted. Considerable research has been done using active techniques such as boundary layer suction (references 1,5,6,7,8) and static devices such as vanes, airfoils, and vortex generators (references 2,3,4,7,9,10,11) to improve the performance of a short diffuser by recovering a higher percentage of the kinetic energy of the flow and reducing the region of flow separation. In diffusers for wind tunnels, wire screens and/or honeycomb structures are used to reduce turbulence and smooth velocity profiles entering the test section. Round-wire screens and sharp-edge-element screens or plates have also been investigated (references 12,13,14,15) as low-loss flow-smoothing devices.

For any grid-type device, including the aforementioned aerogrids of interest here, the principle employed is to size the grid holes to produce a given average subsonic throat velocity for a given average upstream flow condition; if, in any local area, the velocity of the flow impinging on the grid substantially exceeds the average upstream condition, the orifices in that local region will choke the flow and cause a redistribution of flow over the remaining area of the grid. Since the contoured, venturi-type holes in an aerogrid can be designed for a higher average throat velocity for a given pressure drop, this flow-smoothing action becomes more effective than with simple punched plates or screens.

The main objective of the present research effort was to compare the effects of grid blockage (geometric percent solidity in grid throat plane), spacing from diffuser exit plane to grid face, and circumferential and radial (hub- and tip-peaked) distortions in velocity profiles at the diffuser inlet. A second objective was to obtain comparative performance data with simple punched plates.

SYMBOLS

A	flow area
AR	diffuser area ratio = A_2/A_1
M	Mach number
P	static pressure
P_T	total pressure
q	dynamic pressure = $(\gamma/2) \times PM^2$
R	radius from engine centerline
S	solidity = $100\ (A_2 - A_{t_{grid}})/A_2$, percent
V	Velocity
η	diffuser effectiveness = $\dfrac{P_4 - P_1}{q_1(1 - 1/AR^2)}$ (For incompressible flow)
γ	specific heat ratio

Superscript

-	arithmetic average

Subscripts

o	stilling chamber
1	diffuser entrance
2	diffuser exit (dump)
3	upstream of aerogrid or punched plate
4	downstream of aerogrid or punched plate
5	downstream of exit pitot rakes

a	air
avg	average
$\mathfrak{C}_L$	centerline
d	diffuser
i	inner
L	local conditions
max	maximum
o	outer, or open
T	total conditions
t	throat conditions

DESIGN OF DIFFUSER, AEROGRIDS, AND PUNCHED PLATES

Diffuser Design

The critical conditions for designing the diffuser are: 1) the cruise condition, because the pressure loss during cruise must be held to a minimum in the interest of fuel economy, and 2) the most severe condition at which relight might be required, because any flow-smoothing device must not choke (overall) at this condition and thereby further reduce combustor pressure. For the present study the cruise and relight conditions were defined as shown in the upper part of Table I.

TABLE I - DESIGN CONDITIONS AND DIMENSIONS FOR ANNULAR DIFFUSER

Design conditions, diffuser entrance	For Cruise	For Relight
Airflow, $\dot{w}_a$: Full-scale, lb/s (kg/s)	110 (50)	16.5 (7.5)
Model-scale, lb/s (kg/s)	12.2 (5.56)	1.83 (0.833)
Total temperature, T_{T_o}, °F (°C)	1200 (648)	100 (37.8)
Total pressure, P_{T_1}, psia (N/m^2)	90 (6.2×10^5)	6 (4.14×10^4)
Mach number, M_1	0.305	0.434
Dimensions and geometric ratios	**1/3-Scale Model**	**Simulated Full Scale**
Diffuser entrance radii and area:		
R_{i_1}, to inner wall, in. (cm)	4.667 (11.85)	14.00 (35.56)
R_{o_1}, to outer wall, in. (cm)	5.313 (13.50)	15.94 (40.48)
$R_{avg_1} = (R_{i_1} + R_{o_1})/2$, in. (cm)	4.990 (12.67)	14.97 (38.02)
A_1, flow area, $in.^2$ (cm^2)	20.24 (130.6)	182.5 (1177)
Diffuser exit radii and area:		
R_{i_2}, to inner wall, in. (cm)	3.803 (9.66)	11.41 (28.98)
R_{o_2}, to exit wall, in. (cm)	6.428 (16.33)	19.28 (48.97)
$R_{avg_2} = (R_{i_2} + R_{o_2})/2$, in. (cm)	5.116 (12.99)	15.35 (38.98)
A_2, flow area, $in.^2$ (cm^2)	84.49 (545.1)	759.3 (4990)
Diffuser lengths:		
ℓ_d, divergent section, in. (cm)	1.333 (3.39)	4.00 (10.16)
$\ell_{T_{max}}$, total inc. grid, in. (cm)	2.000 (5.08)	6.00 (15.24)
Entrance height/length ratio, $(R_{i_1} - R_{o_1})/\ell_d$	2.07	2.07
Exit/entrance area ratio, A_2/A_1	4.17	4.17

The engine size of interest was one having an annular combustor of approximately 40-inch (102-cm) OD, with a flow area of approximately 5.3 feet^2 (0.5 m^2), preceded by a short annular diffuser with approximately a 4:1 area ratio (exit to inlet) and a length below the 6.6-inch (16.8-cm) length already being used for this engine size. It was decided that the combined length of a new, shorter diffuser and a flow-smoothing grid should not exceed 6 inches (15.2 cm), and that use of 1/3-linear-scale models (having 1/9 the full-scale cross-sectional areas) would provide satisfactory aerodynamic simulations and would permit adequate instrumentation. The model dimensions selected, and the corresponding full-scale dimensions, are given in the lower part of Table I.

Various diffuser designs were considered, and it was decided, based on unreported test data and experience from the Long Range Typhon ramjet work mentioned in the Introduction, to devote 3 in. (7.6 cm) of the 4-in. (10.2-cm) diffuser length ℓ_d to constant-pressure-gradient contours. The last inch (2.5 cm) then would use constant divergence angles to reach the exit radii of the annulus. The contours selected are shown in figures 1 and 2. The features of this design may be stated further as follows:

1) The cruise condition (Table I) is the reference condition.

2) The constant-pressure-gradient section diffuses the flow (theoretically) from Mach 0.3 to Mach 0.2. It has an equivalent conical half-angle of 8.9 degrees.

3) The downstream divergent section, called the dump section, provides adequate radial flow area forward of the grid to ensure unrestricted flow to the outer holes of the aerogrid or punched plate. Provisions were made for testing the grids at two grid-face locations, 0.10 in. (0.25 cm) and 0.25 in. (0.63 cm) downstream from the diffuser exit plane.

Aerogrid Design

Three aerogrids, designated A, B, and C (see figures 3 through 5) were designed in sequence as testing proceeded. The design of aerogrid A was established as follows.

Previous experience with aerogrids indicated that, for good flow distribution with minimum pressure loss, the venturi throat Mach number should be near 0.6 at the design condition. However, for the present application, a compromise was needed between the relight condition (which would choke first because of the lower pressure and lower Reynolds number) and the cruise condition. The Typhon ramjet aerogrid, which had venturis of 0.221-inch (0.56-cm) throat diameter showed a sharp drop in pressure recovery when the throat Reynolds number fell below 30,000. To be conservative, it was decided that aerogrid A should be designed to avoid (by a small margin) choking at a throat Reynolds number of 50,000 at the relight condition.

The desired grid thickness (venturi length) was 1.75 in. (4.44 cm) or less, and a well-shaped venturi has a length/throat-diameter ratio near 4 (see figure 6). Parametric calculations for designs in this vicinity indicated that a design which just choked at the relight condition would have a throat Mach number of 0.52 at the cruise condition. A slight back-off from these values (by an arbitrary 6% increase in throat size) led to the full-scale parameters listed in Table II for aerogrid A.

TABLE II - FULL-SCALE DESIGN PARAMETERS FOR AEROGRID A

Throat Mach number at the relight condition	=	0.76
Throat Mach number at the cruise condition	=	0.48
Hole throat diameter	=	0.383 in.(0.97 cm)
Number of holes	=	1123
Total throat area	=	129.4 in^2 (840 cm^2)

The design of aerogrid B was based on the results obtained from aerogrid A. The target total pressure loss for the diffuser plus aerogrid configuration was 3% at $M_1 = 0.3$. Test data (Run 4) showed that for aerogrid A the total pressure loss for diffuser plus aerogrid was 5.3% (i.e., $\left(\frac{\bar{P}_{T_1} - \bar{P}_{T_4}}{\bar{P}_{T_1}}\right) = 0.053$) at $M_1 = 0.3$, which corresponded to $M_t = 0.48$. Calculations at these conditions showed a divergence loss from the venturis, $\left(\bar{P}_{T_3} - \bar{P}_{T_4}\right)/q_t$, of 0.167. Since $\left(q/P_T\right)_t = 0.138$ at $M_t = 0.48$, and $\bar{P}_{t_3} \simeq \bar{P}_{T_t}$, this yields the following estimated total pressure loss across aerogrid A:

$$\left(\bar{P}_{T_3} - \bar{P}_{T_4}\right)/\bar{P}_{T_t} \simeq \left(\bar{P}_{T_3} - \bar{P}_{T_4}\right)/q_t \times \left(q/P_T\right)_t = 0.167 \times 0.138 = 0.023.$$

By difference the estimated loss for the diffuser was 0.053 - 0.023 = 0.03, or 3%.

Since the overall total pressure loss of 5.3% for aerogrid A was unacceptably high, aerogrid B was designed to have a grid throat Mach number of 0.3, such that $\left(q/P_T\right)_t = 0.059$. Using the same estimate for divergence loss (0.167) as was used for aerogrid A, the estimated total pressure loss across aerogrid B was (0.167)(0.059) = 0.0098, or less than half that for aerogrid A. The corresponding throat diameter for aerogrid B was 0.155 in. (0.393 cm), or 1.125 times that of aerogrid A. Figure 6 specified the venturi contours for aerogrids A and B.

Aerogrid C (Figure 5) was designed to reduce further the total pressure loss and flatten the parabolic exit velocity profile exhibited by grid B. The central core holes were kept at the 0.155 in. (0.393 cm) diameter specified for grid B, but the inner and outer holes were enlarged to 0.240-in. (0.609-cm) diameter, so that the flow would spread more to the inner and outer holes.

Table III summarizes the design specifications for the three 1/3-scale aerogrid models.

TABLE III

SPECIFICATIONS FOR 1/3-SCALE AEROGRID MODELS
Each has 1123 holes and is 0.487 in.(1.237 cm) thick

Parameter	Aerogrid A	Aerogrid B	Aerogrid C
Throat diameter, in.(cm)	0.1277(0.324)	0.155(0.394)	0.155(0.394)[a] 0.250(0.610)[b]
Throat area, A_t(1123 venturis), in.^{2} (cm^2)	14.34 (92.5)	21.6 (139.4)	33.32 (215.0)
Percent blockage, $\frac{A_2 - A_t}{A_2} \times 100$	83	74	61

[a] For 460 central core holes (midway in annulus)

[b] For 663 inner and outer holes (total, a + b = 1123 holes)

Punched Plate Design

Punched plates A and B (Figures 7 and 8, respectively) were designed to have the same total pressure losses as aerogrids A and B, respectively, at $M_1 = 0.3$. The number of holes (1123) and hole pattern were kept the same as those of the aerogrids. The theory developed in reference 15 for low-velocity flow through sharp-edged orifices was used. For punched plate A, the loss coefficient, $\left(\bar{P}_{T_3} - \bar{P}_{T_4}\right)/q_3$, was calculated as follows:

At $M_1 = 0.3$, $M_3 = 0.072$, and $q/P_{T_3} = 0.0036$. To match the 2.3% total pressure loss of aerogrid A,

$$\frac{\left(\bar{P}_{T_3} - \bar{P}_{T_4}\right)}{q_3} = \frac{\bar{P}_{T_3} - \bar{P}_{T_4}}{\bar{P}_{T_3}} \cdot \frac{1}{\left(q/P_T\right)_3} = \frac{0.023}{0.0036} = 6.5$$

This loss coefficient corresponds (per ref. 15) to a blockage of 58% yielding a hole diameter of 0.200 inch (0.508 cm) for punched plate A.

In a like manner, punched plate B was designed to match the total pressure loss of 0.98% at M_1 = 0.3 for aerogrid B. The loss coefficient was computed to be 0.86, which required a blockage of 30% and a hole diameter of 0.259 inch (0.657 cm).

No punched plate C was designed because the test results for aerogrid C showed no improvement over aerogrid B, leaving no reason to fabricate a third punched plate.

TEST APPARATUS AND INSTRUMENTATION

Flow System

Figure 9 shows the overall experimental setup. Air is supplied to the connected pipe test rig at pressures from 1200 to 125 psia (8.3×10^6 to 0.9×10^6 N/m^2) and at ambient temperatures from remotely located air storage tanks. The airflow to the model is controlled by a choked ASME long-radius nozzle. The range of test Reynolds numbers is controlled by scheduling various airflow rates. At each airflow, the pressure level in the model is varied by restricting the model exit in order to obtain the desired range of inlet Mach numbers (0.15 to 0.45). With a choked nozzle upstream of the model controlling the inlet airflow rate, choked ASME long-radius nozzles at the exit provide an accurate means of controlling the pressure level in the model at constant inlet airflow rates.

For the high airflows, 18 and 11 lb/sec (8.2 and 5.0 kg/sec), the air discharging from the diffuser is exhausted to the atmosphere. For the low airflows, 2 and 3 lb/sec (0.91 and 1.36 kg/sec), the exhaust is connected to a steam ejector, which produces the required vacuum to ensure that the exit nozzles are choked.

Uniform, low-velocity flow was produced in the stilling chamber upstream of the diffuser by use of a central baffle plate immediately downstream of the inlet nozzle, and a 36%-open-area screen attached to radial support arms (resulting in a net 26 percent open flow area) at the entrance to the stilling chamber.

The test section (approximately 7.8 feet (2.4 m) in length) is composed of five cylindrical pipe segments which begin at the airflow nozzle exit plane and end downstream of the aerogrid exit station. The diffuser and aerogrid assembly is contained in a 14-inch (35.56-cm)-OD x 3/4-inch (1.90-cm)-wall steel pipe which is held between the inlet stilling chamber section and the diffuser exhaust section by two grooved pipe joint clamps. In addition to several clamps, the segmented test rig is held rigidly in alignment by three one-inch-diameter steel draw bars.

Distortion Elements

Two types of inlet flow distortion were used to evaluate the ability of an aerogrid to smooth distorted flow. A circumferential distortion was generated by placing a 10° sector of 36% open wire screen across

the two inlet bellmouth sections at the 3 o'clock circumferential location. This sector of screen produced a uniform, 25% lower than average, velocity profile across the inlet annular gap at 3 o'clock while not affecting the inlet velocity profile at either the 9 or 12 o'clock positions. It was designed to be manually rotated into position and was used with both the aerogrids and punched plates.

The second type of inlet flow distortion was a hub- or tip-peaked radial profile generated by removing one or the other of the elliptically-shaped bellmouth rings attached at the leading edge of the inlet annulus, thereby forcing a slower flow into the inlet on the side from which the bellmouth section was removed. Both hub- and tip-peaked inlet flow distortions were investigated. Both of these radial distortions produced velocity profiles with differences between maximum and minimum points of approximately 40%.

Instrumentation

The total and static pressure measurements, with the exception of two reference pressures, were made using scanivalves and differential pressure transducers. For maximum accuracy in the data, much effort was spent in accurately establishing the pressure rise time in relation to the switching rate in the scanivalves and matching as closely as possible the differential range between the reference pressures and the sample pressures to the ranges of commercially available differential pressure transducers.

The instrumentation list is shown in Appendix A, Table A-I. The first column indicates station number, where appropriate, and the second column shows equivalent full-scale axial locations relative to the diffuser entrance (station 1). Some circumferential locations were offset slightly from the nominal o'clock positions to avoid wake interference between upstream and downstream rakes.

As shown in figure 1, three total pressure rakes were used at the diffuser inlet with probes spaced radially to provide an area-weighted average total pressure. These rakes were located 1 in. (2.54 cm) upstream from the beginning of the diffuser entrance (station 1) and were considered to represent total pressure at station 1. A five-probe rake was located at the 12 o'clock position circumferentially, and three-probe rakes were located at 3 o'clock and 9 o'clock, respectively. All of these probes were connected to a 48-port scanivalve. There were eleven primary pressures and one reference pressure, each of which was manifolded to four ports in order to fill the 48-port capacity of the scanivalve. The other side of the scanivalve was connected to a 15-psid (1×10^5 N/m^2) differential-pressure transducer on the high-pressure side, and the reference pressure was connected to the low-pressure side of the same transducer. Therefore, all inlet total pressures were read as differential pressures referenced to the static pressure in the vicinity of the 12 o'clock rake position at station 1.

The absolute value of the primary reference pressure (the stilling chamber static pressure at station 0 in figure 1) was measured by a

0-250 psi (0-1.7 x 10^6 N/m^2) strain-gage type pressure transducer. Each of the scanivalve reference pressures was then determined by measuring the differential pressure between the desired reference pressure and the primary reference pressure and then subtracting that differential pressure from the primary reference pressure.

The diffuser wall static pressures were connected in a like manner to a scanivalve and a 15-psid (1 x 10^5 N/m^2) differential-pressure transducer. The reference pressure for all wall static pressures was the 3 o'clock stilling chamber static pressure (which was connected to the high-pressure side of the transducer).

The diffuser exit total pressures were measured using three total-pressure rakes, a ten-probe rake at 12 o'clock, and five probe rakes at 3 o'clock and 9 o'clock, with the probes radially spaced so as to provide an area-weighted average total pressure. All three exit rakes were located axially at station 10, referenced to full scale. They were connected to a scanivalve and a 1-psid (7 x 10^3 N/m^2) differential pressure transducer. For tests with no flow resistance upstream of the rakes, i.e., no aerogrid or punched plate, a 10-psid (7 x 10^4 N/m^2) transducer was used in place of the 1-psid (7 x 10^3) unit. The reference pressure for this unit was the outer wall static in the vicinity of the 12 o'clock rake at the same axial location.

The stilling chamber static pressures, the airflow nozzle inlet pressures, and the model outlet wall static pressures were measured using strain-gage-type absolute pressure gages.

The six probes of the boundary-layer rake (also shown in figure 1) and the adjacent wall-static probe used as the rake reference pressure were individually connected to seven solenoid valves, all of which were manifolded to a 6-psid (4 x 10^4 N/m^2) differential pressure transducer. The boundary-layer rake was positioned at 6 o'clock at station 1, the beginning of the diffuser divergence.

The airflow nozzle inlet temperatures, the stilling chamber air temperatures, and the model outlet air temperatures were measured with chromel/alumel thermocouples.

Performance Parameters

The local velocity at each pitot probe position was computed by using the measured rake pitot pressure, the measured static pressure on the body at the rake station (thereby assuming a uniform static pressure distribution across the annular sections), and a local-to-total temperature ratio based on the Mach number calculated from the measured static-to-total pressure ratio at each rake probe. Each local velocity V_L was then normalized by dividing by the arithmetic average V_{avg} of all velocities computed for that rake. To illustrate the circumferential distortion produced by the 10°

sector screens, however, V_L's for the 3 o'clock station (in the wake of the screens) were normalized by V_{avg} for the 12 o'clock station.

The overall total pressure recovery of the diffuser and flow resistance element was computed as the ratio of the mass-weighted total pressures at the exit rake to that of the inlet rake. For diffuser-alone tests, a single static tap at the dump station, the area at that station, and the computed inlet mass flow, were used to determine the total pressure at the diffuser exit.

RESULTS AND DISCUSSION

Test Variable Ranges

Twenty test runs were made at the blow-down facility of the Propulsion Research Laboratory at APL. The principal test variables, diffuser inlet Mach number and Reynolds number, were varied over the ranges $0.15 < M_1 < 0.45$ and $60 \times 10^3 < Re < 675 \times 10^3$, respectively. Because the velocity profiles were found to be insensitive to Mach number, as illustrated in figure 10, most of the comparisons presented hereinafter are for a diffuser inlet Mach number of approximately 0.3.

The test matrix is shown in Appendix A, Table A-II. Two grid-face positions were tested (refer to figure 2). The "forward position" was 0.10 in. (0.254 cm) downstream from station 2 (diffuser dump plane), and the "aft position" was 0.25 in. (0.635 cm) downstream from station 2.

Results for Aerodynamic Grids at the Forward Position

Aerogrid A produced a very flat but slightly inverted (higher velocities at the wall than in the core) exit velocity profile. However, as previously noted, the overall total pressure loss at $M_1 = 0.3$ of 5.3% was unacceptably high, therefore aerogrid B was designed and tested. The latter was theoretically designed to have a 1% total pressure drop across the grid. When it was tested with the diffuser, the measured overall total pressure loss was 3% at $M_1 = 0.3$. However, due to its decreased solidity, its exit velocity profile was parabolic -- not as flat as the profile from grid A -- and the peak of the profile was skewed toward the inner wall, as seen in figure 11.

For aerogrid C, which had larger outer and inner holes than aerogrid B as previously discussed, the exit velocity profile (figure 12) was more peaked, and the flow separated across the outer ten percent of the annular height. Therefore, this design was eliminated from further testing.

Effect of Distorted Inlet Flow

At the inlet to the diffuser, the 10° sector, wire-screen, radial element produced a circumferential distortion of uniform 25% lower velocity

across the inlet height at 3 o'clock while not affecting the inlet velocity profile at either the 9 or 12 o'clock positions (figure 13). Figures 14 and 15 show the efficiency of aerogrids A and B (at the forward position) in smoothing this circumferential distortion. The curves for the 3 o'clock rake behind each aerogrid (velocities normalized to V_{avg} for the 12 o'clock rake) show that aerogrid A effectively smoothed most of the wake generated by the circumferential distortion element (figure 14). In contrast, the 3 o'clock rake behind aerogrid B indicated essentially zero velocity, i.e., a region of separated flow still persisted (figure 15).

In figure 13 the inlet profiles of tip- and hub-peaked radial distortion are also shown. The minimum velocity for both of these radial distortions is approximately 40% less than the maximum velocity. Only aerogrid B was tested (at the forward position) with these radial distortions. Fig. 16 shows how it smoothed a tip-peaked radial distortion, which in an open duct produced a separated flow in the innermost 60% of the annulus height. With aerogrid B, the exit flow profile was relatively smooth and parabolic, with flow separation only on the innermost 10% of the annulus height. Fig. 17 illustrates the smoothing achieved for a hub-peaked radial distortion; it presents almost a mirror-image duplication of the smoothing of the tip-peaked distortion. Figure 18 compares the regular, tip-peaked and hub-peaked profiles downstream of aerogrid B.

Comparison of Results for Punched Plates and Aerodynamic Grids

Theoretically, punched plates A and B were designed to have the same total pressure drops as aerogrids A and B, respectively (in the forward position) at $M_1 = 0.3$ (fig. 19). The test results shown in figure 20 summarize the overall pressure loss characteristics of the aerogrids and punched plates and compare them to the diffuser-alone pressure loss. Fig. 21 presents the same results in terms of the comparison of the diffuser-effectiveness η, which is defined as the ratio of the actual to the ideal increase in static pressure of the air passing through the diffuser. It should be noted here that the diffuser effectiveness parameter, η, was derived for incompressible flow. The test data presented in figure 21 were calculated using the incompressible equation. Accounting for compressibility would increase the effectiveness from approximately one to five percent for inlet Mach numbers of 0.15 to 0.45, respectively. In this report the effect of compressibility in the diffuser effectiveness parameter is neglected. It would be expected, of course, that an open duct contoured over the full available length (including the length occupied by a grid in these tests) would have had a higher effectiveness than this shortened diffuser; however, it would not have smoothed the flow as the grids do. At the target point ($M_1 = 0.3$) both aerogrid A and punched plate A exhibited overall total pressure losses of approximately 5.3%, which exceeds the required 3% or lower total pressure loss goal. Punched plate B and aerogrid B both have less pressure loss than an open duct and both meet the required 3% loss at $M_1 = 0.3$.

Figure 22 illustrates the typical Reynolds number effect on the contoured venturis of an aerogrid as opposed to this effect on the simple orifices of a punched plate. This figure bears out the design philosophy for aerogrid A which was designed for a throat Reynolds number of 50,000. As the throat Reynolds number drops below design, the total pressure recovery decreases rapidly (i.e., total pressure loss increases). By contrast, the punched plate shows only a very slight influence of Reynolds number on its performance.

For corresponding total pressure losses at the target point, figures 23 and 24 show that the punched plates were much less effective in smoothing the flow than the corresponding aerogrids. The punched plates were only tested in the forward position (0.10 in., 0.254 cm) to compare to the better grid performance.

Effect of Grid Position

As previously mentioned, the aerogrids were tested at 0.10 and 0.25 inches (0.254 cm and 0.635 cm) aft of the diffuser exit plane. Figures 25a, 25b, and 26 show that the position effect (on total pressure loss and flow smoothing) was small for aerogrid B, but results were slightly better for the forward (0.10-in.) (0.254-cm) position. Aerogrid A, however, showed a noticeable improvement in flow smoothing when positioned closest to the diffuser exit plane (figure 27).

Summary Figure - Velocity Profiles

Figure 28 summarizes the profiles produced for aerogrids A and B and punched plates A and B, all at the forward position, and the open duct.

SUMMARY OF RESULTS

Pressure recoveries and velocity profiles relating to the flow-smoothing capabilities of aerodynamic grids and punched plates coupled to a short, annular diffuser were measured in a series of test runs. The results were as follows:

1. Aerogrid B, with 74% geometric blockage, and punched plate B, with 30% geometric blockage (48% effective blockage), met the target overall pressure loss (diffuser plus grid) of 3% for a diffuser inlet Mach number of 0.3.

2. For equal overall total pressure losses, the aerogrids produced much better velocity profiles than the punched plates.

3. Considering also the ability of aerogrid B to smooth radially-distorted inlet flows, it clearly was the best configuration tested.

4. The aerogrids gave better pressure recovery and smoother velocity profiles when placed 0.10 in. (0.254 cm) from the exit of the short, annular diffuser than when 0.25 in. (0.625 cm) from it.

5. Only aerogrid A was able to reduce substantially the circumferential distortion introduced by a 10° sector of blockage screen, but aerogrid A produced too high a pressure loss (5.3% for diffuser plus grid) to be of interest.

REFERENCES

1. Juhasz, A.J., and Holdeman, J.D.: Preliminary Investigation of Diffuser Wall Bleed to Control Combustor Inlet Airflow Distribution. NASA TN D-6435, July 1971.

2. Henry, J.R., Wood, C.C., and Wilbur, S.W.: Summary of Subsonic-Diffuser Data. NACA RM L56F05, October 1956.

3. Woollett, R.R.: Preliminary Investigation of Short, Two-Dimensional Subsonic Diffusers. NACA RM E56C02, May 1956.

4. Wood, C.C. and Higginbotham, J.T.: Effects of Diffuser and Center-Body Length on Performance of Annular Diffusers with Constant-Diameter Outer Walls and with Vortex-Generator Flow Controls. NACA RM L54G21, September 1954.

5. Wilbur, S.W. and Higginbotham, J.T.: Investigation of Two Short Annular Diffuser Configurations Utilizing Suction and Injection as a Means of Boundary-Layer Control. NACA RM L54K18, January 1955.

6. Wood, C.C. and Higginbotham, J.T.: Flow Diffusion in a Constant-Diameter Duct Downstream of an Abruptly Terminated Center Body. NACA RM L53D23, July 1953.

7. Henry, J.R., and Wilbur, S.W.: Preliminary Investigation of the Flow in an Annular-Diffuser - Tailpipe Combination with an Abrupt Area Expansion and Suction, Injection, and Vortex-Generator Flow Control. NACA RM L53K30, February 1954.

8. Wilbur, S.W. and Higginbotham, J.T.: Investigation of a Short-Annular-Diffuser Configuration Utilizing Suction as a Means of Boundary-Layer Control. NACA TN 3996, June 1957.

9. Farley, J.M. and Welna, H.J.: Investigation of Conical Subsonic Diffusers for Ram-Jet Engines. NACA RM E53L15, March 1954.

10. Valentine, E.F. and Carroll, R.B.: Effects of Some Primary Variables of Rectangular Vortex Generators on Static Pressure Rise through a Short Diffuser. NACA RM L52B13, 1954.

11. Valentine, E.F. and Carroll, R.B.: Effects of Several Arrangements of Rectangular Vortex Generators on the Static-Pressure Rise through a Short 2:1 Diffuser. NACA RM L50L04, February 1951.

12. Schubauer, G.B. and Spangenberg, W.G.: Effect of Screens in Wide-Angle Diffusers. NACA TN 1610, July 1948.

13. Adler, A.A.: Variation with Mach Number of Static and Total Pressures through Various Screens. NACA CB L5F28.

14. Davis, G. DeVahl: The Flow of Air Through Wire Screens. Proceedings of 1st Australian Conference held at the University of West Australia. Edited by R. Silvester, Hydraulics and Fluid Mechanics, 1964 Pergammon, Macmillan.

15. Cornell, W.G.: Losses in Flow Normal to Plane Screens. Presented at the Fall Meeting of the ASME. Paper No. 57-F-19. September 1957.

16. Truly, R.H., et al: Supersonic Diffuser with Shock Positioning Means. Patent #2,968,147 to Boeing Airplane Company, Seattle, Washington. Patented January 17, 1961.

APPENDIX A

TABLE A-I INSTRUMENTATION LIST

Station	Equivalent full-scale axial location [a]	Circumferential location(s) O'clock position(s)	Function description	Instrument range
---	---	3, 9	Airflow nozzle inlet wall static pressure	0-3000 psia ($0-21 \times 10^6$ N/m^2)
---	---	6, 12	Airflow nozzle inlet temperature	-50° to 100°F (228° to 311°K)
0	---	3, 9	Stilling chamber wall static pressure	0-250 psia (0.17×10^6 N/m^2)
0	---	2, 10	Stilling chamber air temperature	-50° to 100°F (228° to 311°K)
(1)[a]	-3	12, 3:20, 9:20	Inlet rake wall static differential pressure	0-15 psid (1×10^5 N/m^2)
(1)[a]	-3	11:45	Inlet rake pressures[b], probes 1 through 5	0-15 psid (1×10^5 N/m^2)
(1)[a]	-3	3, 9	Inlet rake pressures[b], probes 1, 3, 5	0-15 psid (1×10^5 N/m^2)
1	0	12	Diffuser outer wall static differential pressure	0-15 psid (1×10^5 N/m^2)
---	+1	12, 3:20, 9:20	Diffuser outer wall static differential pressure	0-15 psid (1×10^5 N/m^2)
---	+2	12, 3:20, 9:20	Diffuser outer wall static differential pressure	0-15 psid (1×10^5 N/m^2)
2	+4	12	Diffuser outer wall static differential pressure	0-15 psid (1×10^5 N/m^2)
3	+10	12, 3:20, 9:20	Diffuser outer wall static differential pressure	0-15 psid (1×10^5 N/m^2)

(cont'd.)

Station	Equivalent full-scale axial location[a]	Circumferential location(s) / 0'clock position(s)	Function description	Instrument range
4	+10	12:15	Diffuser exit rake differential[b] pressures, probes 1-10	0-1 psid (0.7×10^4 N/m^2)
4	+10	3, 9	Diffuser exit rake differential[b] pressures, probes 1, 3, 6, 8, 10	0-1 psid (0.7×10^3 N/m^2)
5	+24		Model outlet wall static pressure	0-250 psia ($0-1.7 \times 10^6$ N/m^2)
5	+24	2, 10	Model outlet air temperature	-50 - 100 F (228° to 311°K)
1	0	6	Boundary-layer rake pressures[b], probes 1-6	0-6 psid (0.4×10^4 N/m^2)
5	72	4:30	Model exit static pressure[c] (outer model wall)	CEC[c]
0		3:20	Reference differential pressure, scani Ref	0-15 psid (1×10^5 N/m^2)
(1)[a]	-3	12:30	Ref. diff. press., scanivalve #1	0-15 psid (1×10^5 N/m^2)
2	+10	11:40	Ref. diff. press., scanivalve #3	0-15 psid (1×10^5 N/m^2)
(1)[a]	-3	12:30	Ref. diff. press., PMUX #4	0-6 psid (0.4×10^4 N/m^2)
---	---	---	Exhaust header static pressure	0-25 psia ($0-1.7 \times 10^5$ N/m^2)

[a] Location relative to diffuser entrance station 1; e.g., -3 is 3 in. (7.6 cm) upstream from station 1 (but is assumed to represent station 1), or +4 is 4 in. (10.1 cm) downstream from station 1.

[b] Rake differential pressure = (probe total pressure) - (wall static pressure).

[c] High response, close-coupled transducer recorded on oscillograph, 0-500 psia 0-3.5×10^6 N/m^2).

APPENDIX A

TABLE A-II ANNULAR DIFFUSER TEST MATRIX

Run	Configuration	Position of diffuser	Configuration variables	Test mass flow lbs/sec(kg/sec)
1	Aerogrid A	0.25 in.(0.635 cm)	----	17, 11, 2, 3 (7.7,5,0.9,1.4)
2	Open duct (no resistance)	----	----	18, 11 (8.2, 5)
3	Open duct (no resistance)	----	Radial blockage @ 3 o'clock	9, 3 (4.1, 1.4)
4	Aerogrid A	0.10 in.(0.254 cm)	----	18, 11, 2, 3 (8.2,5,0.9,1.4)
5	Aerogrid A	0.10 in.(0.254 cm)	Radial blockage @ 3 o'clock	18, 11, 2, 3 (8.2,5,0.9,1.4)
6	Aerogrid B	0.10 in.(0.254 cm)	----	18, 11, 2, 3 (8.2,5,0.9,1.4)
7	Aerogrid B	0.25 in.(0.635 cm)	----	18, 11, 2, 3 (8.2,5,0.9,1.4)
8	Aerogrid B	0.10 in.(0.254 cm)	Radial blockage @ 3 o'clock	18, 11, 2, 3 (8.2,5,0.9,1.4)
9	Punched plate A	0.10 in.(0.254 cm)	----	18, 11, 2, 3 (8.2,5,0.9,1.4)
10	Punched plate A	0.10 in.(0.254 cm)	Radial blockage @ 3 o'clock	18, 11, 2, 3 (8.2,5,0.9,1.4)
11	Punched plate B	0.10 in.(0.254 cm)	----	18, 11, 2, 3 (8.2,5,0.9,1.4)
12	Punched plate B	0.10 in.(0.254 cm)	Radial blockage @ 3 o'clock	18, 11, 2, 3 (8.2,5,0.9,1.4)
13	Aerogrid C	0.10 in.(0.254 cm)	----	18, 11, 2, 3 (8.2,5,0.9,1.4)
14	Aerogrid C	0.10 in.(0.254 cm)	Radial blockage @ 3 o'clock	18, 11, 2, 3 (8.2,5,0.9,1.4)

Run	Configuration	Position aft of diffuser	Configuration variables	Test Mass flow lbs/sec(kg/sec)
15	Aerogrid B	0.10 in.(0.254 cm)	Tip-peaked inlet profile	18, 11, 2, 3 (8.2,5,0.9,1.4)
16	Aerogrid B	0.25 in.(0.635 cm)	Tip-peaked inlet profile	18, 11, 2, 3 (8.2,5,0.9,1.4)
17	Aerogrid B	0.10 in.(0.254 cm)	Hub-peaked inlet profile	18, 11, 2, 3 (8.2,5,0.9,1.4)
18	Open duct (no resistance)	----	Hub-peaked inlet profile	18, 11, 2, 3 (8.2,5,0.9,1.4)
19	Open duct (no resistance)	----	Tip-peaked inlet profile	18, 11, 2, 3 (8.2,5,0.9,1.4)
20	Aerogrid B	0.10 in.(0.254 cm)	12 o'clock exit moved to 0.45 in. (1.38 cm) aft of grid	18, 11, 2, 3 (8.2,5,0.9,1.4)

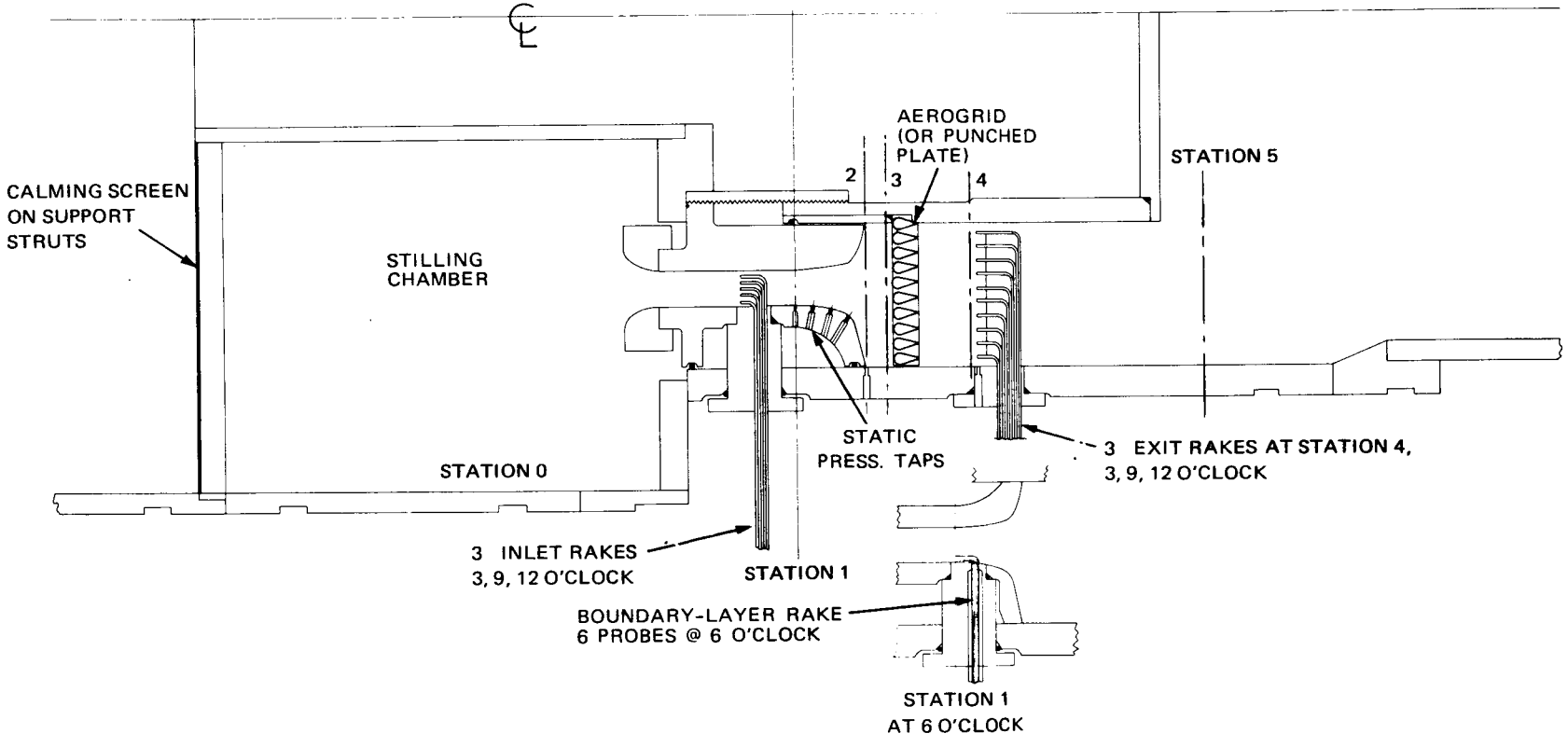

Figure 1 DIFFUSER TEST APPARATUS AND PRESSURE INSTRUMENTATION

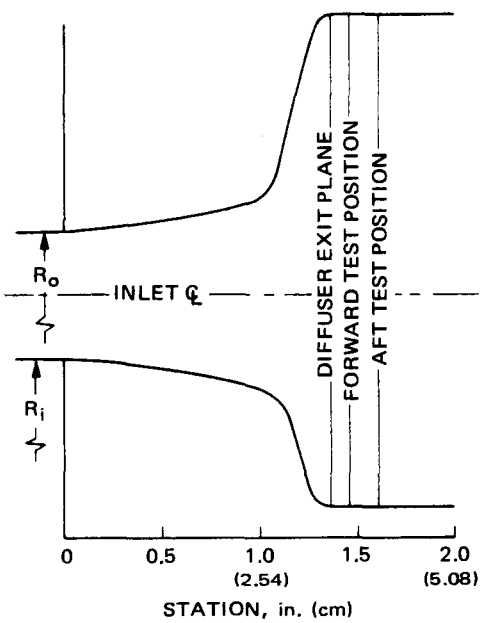

COORDINATES FOR 1/3 –SCALE SUBSONIC DIFFUSER

STATION		R_i		R_o	
in.	(cm)	in.	(cm)	in.	(cm)
0	0	4.667	11.854	5.313	13.495
0.167	0.424	4.652	11.816	5.328	13.533
0.250	0.635	4.643	11.793	5.337	13.556
0.417	1.059	4.624	11.745	5.356	13.604
0.500	1.270	4.612	11.714	5.368	13.635
0.667	1.694	4.586	11.648	5.394	13.701
0.833	2.116	4.553	11.565	5.427	13.785
1.000	2.540	4.510	11.455	5.470	13.894
1.033	2.624	4.503	11.438	5.493	13.952
1.067	2.710	4.483	11.387	5.533	14.054
1.100	2.794	4.453	11.311	5.640	14.326
1.133	2.878	4.407	11.194	5.780	14.681
1.167	2.964	4.287	10.889	5.917	15.029
1.267	3.218	3.887	9.873	6.327	16.071
1.300	3.302	3.823	9.710	6.400	16.256
1.333	3.386	3.803	9.660	6.420	16.307
1.367	3.472	3.800	9.652	6.427	16.324

DIFFUSER EXIT PLANE AT STATION 1.367 IN. (3.472 cm)
FORWARD TEST POSITION AT STATION 1.467 IN (3.726 cm)
AFT TEST POSITION 1.617 IN. (4.107 cm)

Figure 2 DIFFUSER CONTOUR AND AEROGRID (OR PUNCHED PLATE) TEST POSITIONS

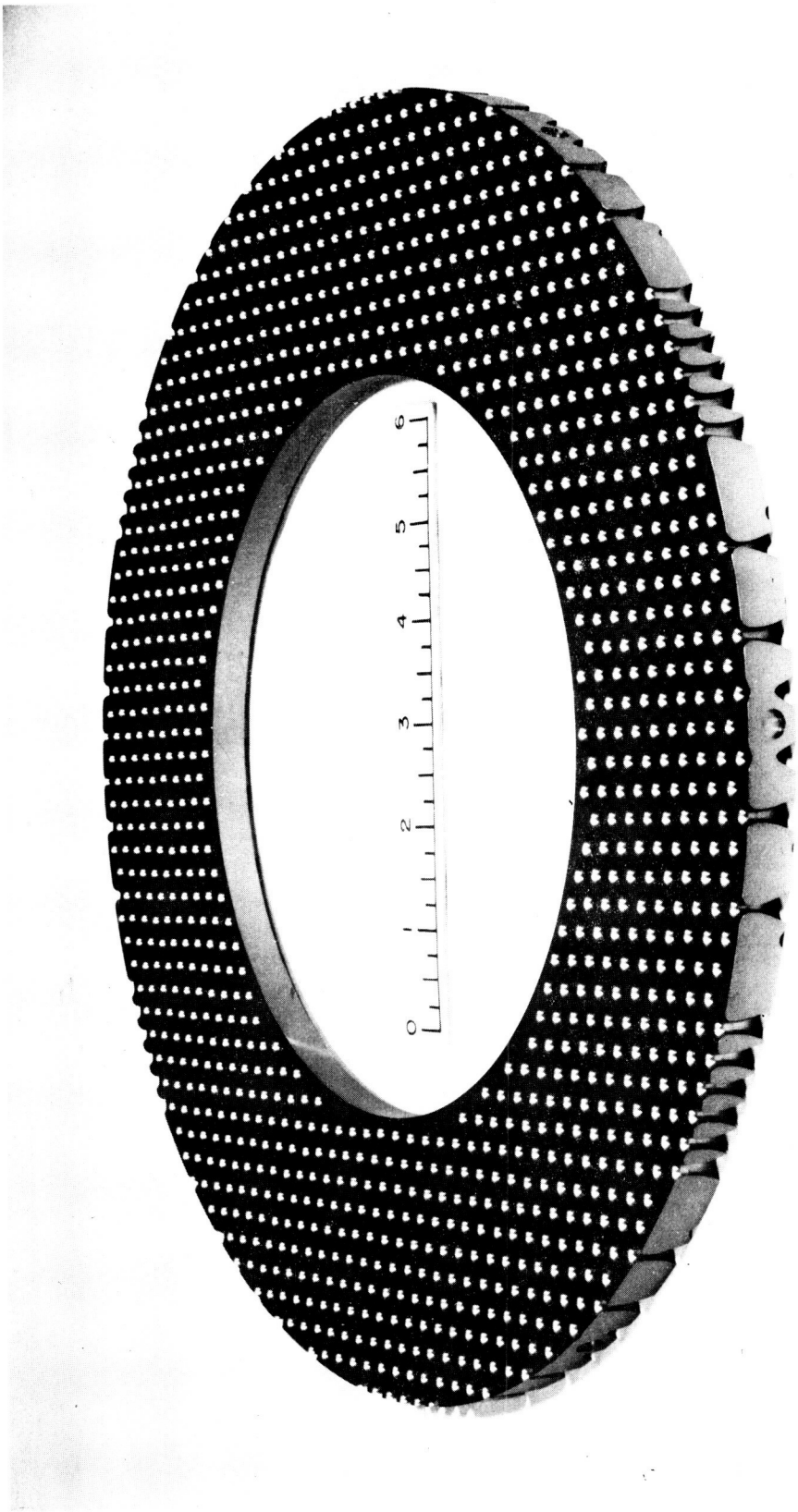

Figure 3 AEROGRID A, 17% OPEN AREA

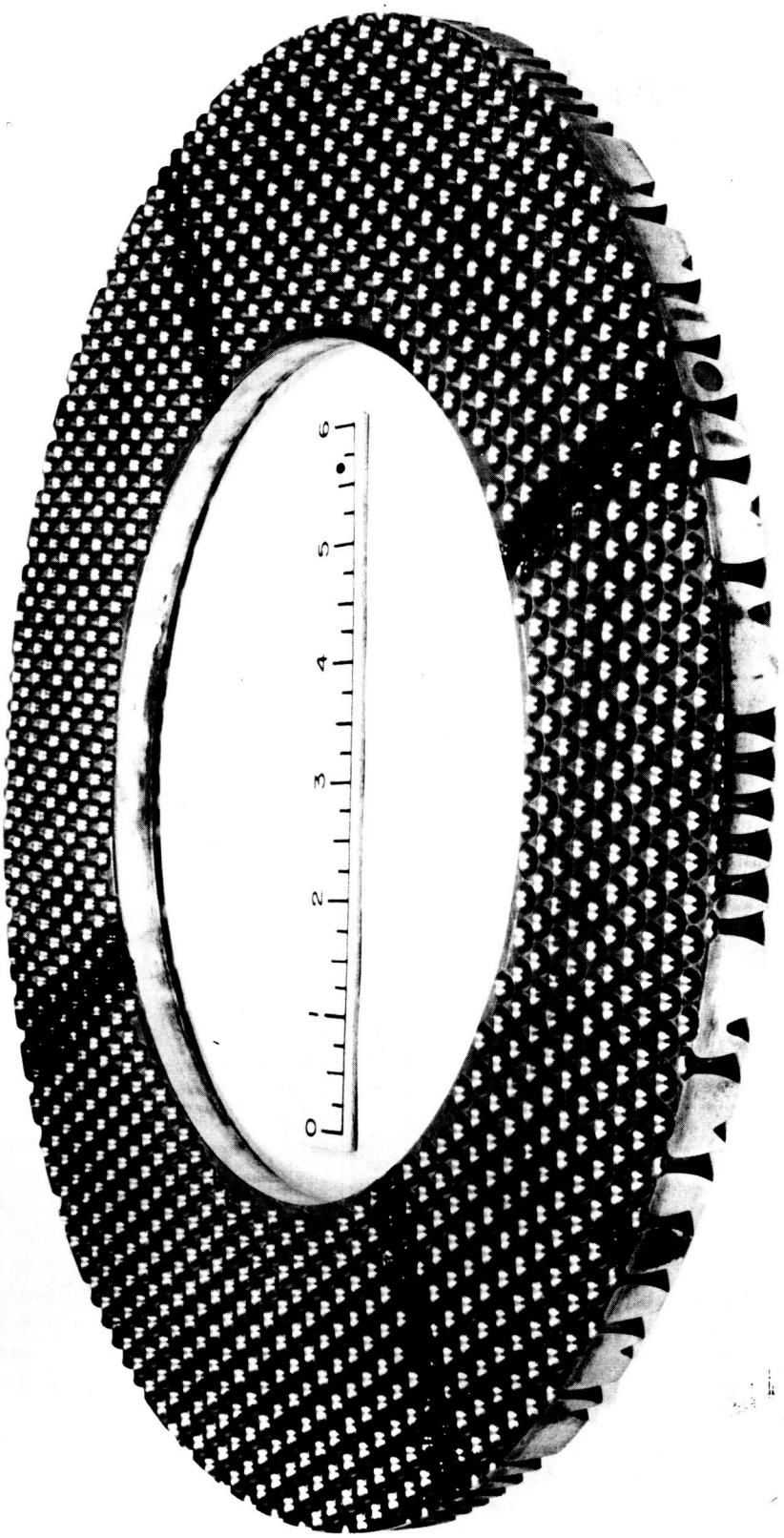

Figure 4 AEROGRID B, 26% OPEN AREA

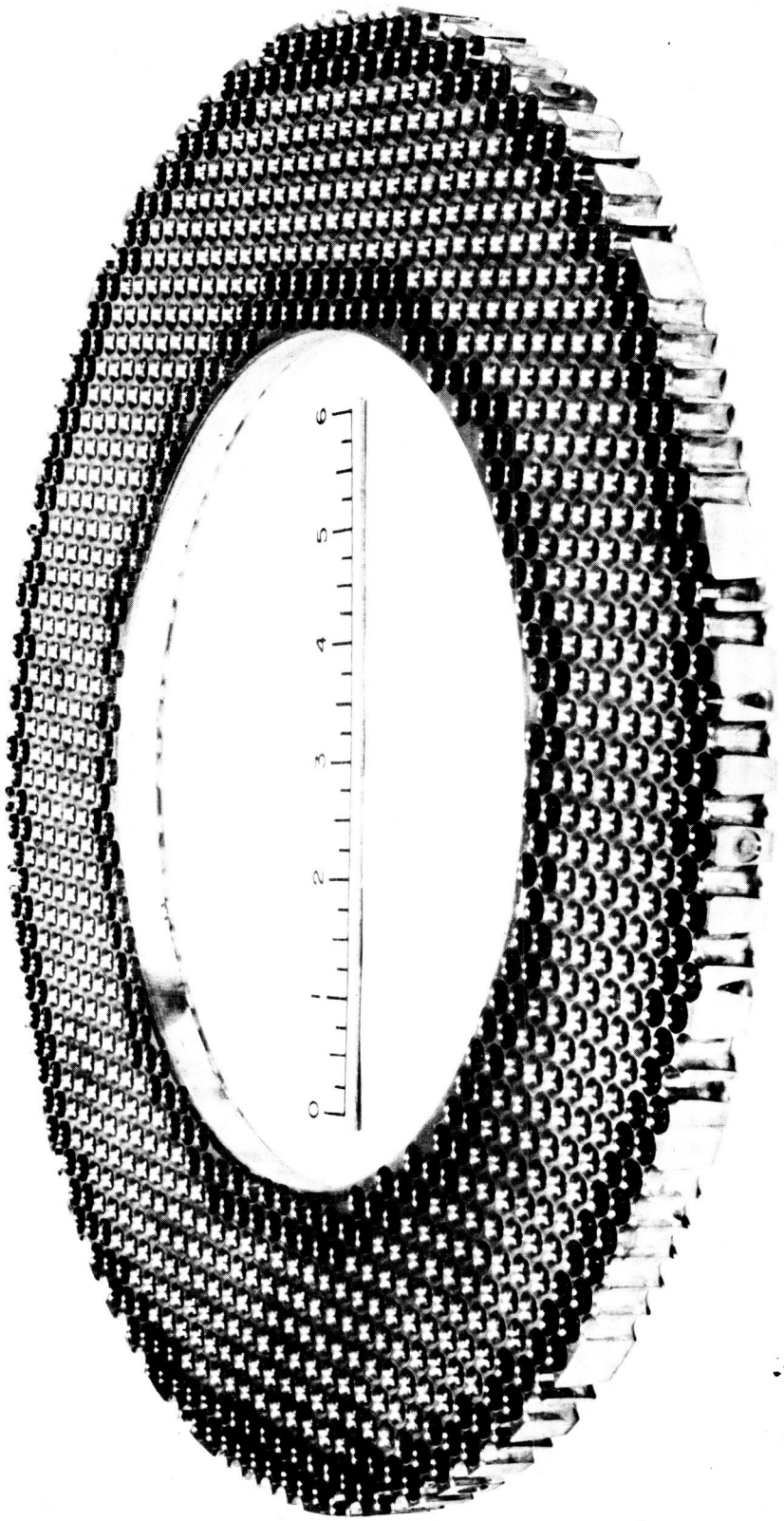

Figure 5 AEROGRID C, 39% OPEN AREA

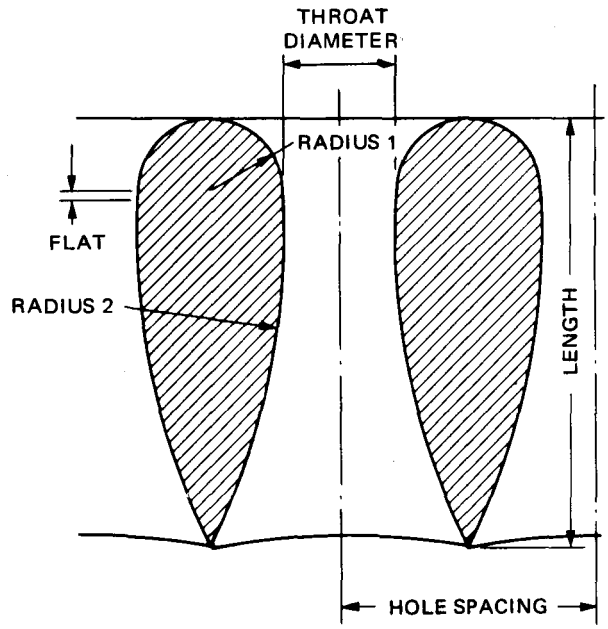

	AEROGRID A	AEROGRID B
RADIUS 1	0.0803 in. (0.2040 cm)	0.06975 in. (0.1772 cm)
RADIUS 2	0.7989 in. (2.0292 cm)	1.23075 in. (3.1261 cm)
THROAT DIAMETER	0.1277 in. (0.3244 cm)	0.1551 in. (0.3939 cm)
HOLE SPACING	0.2946 in. (0.7483 cm)	
FLAT	0.0083 in. (0.0211 cm)	
LENGTH	0.4865 in. (1.2357 cm)	

Figure 6 NASA TURBOJET AEROGRID HOLE CONTOUR (MODEL DIMENSIONS SHOWN 1/3 FULL SCALE)

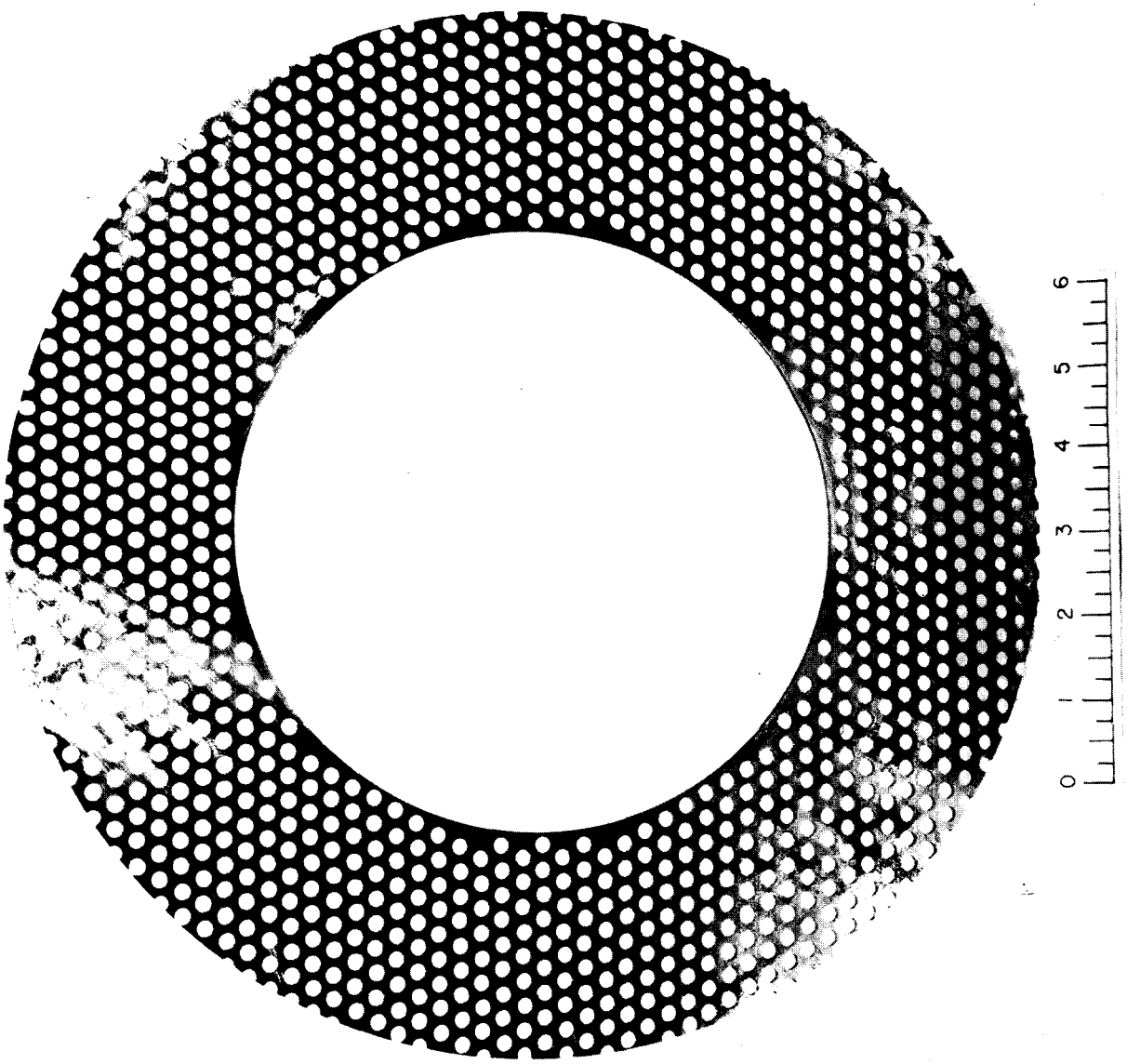

Figure 7 PUNCHED PLATE A, 42% OPEN AREA

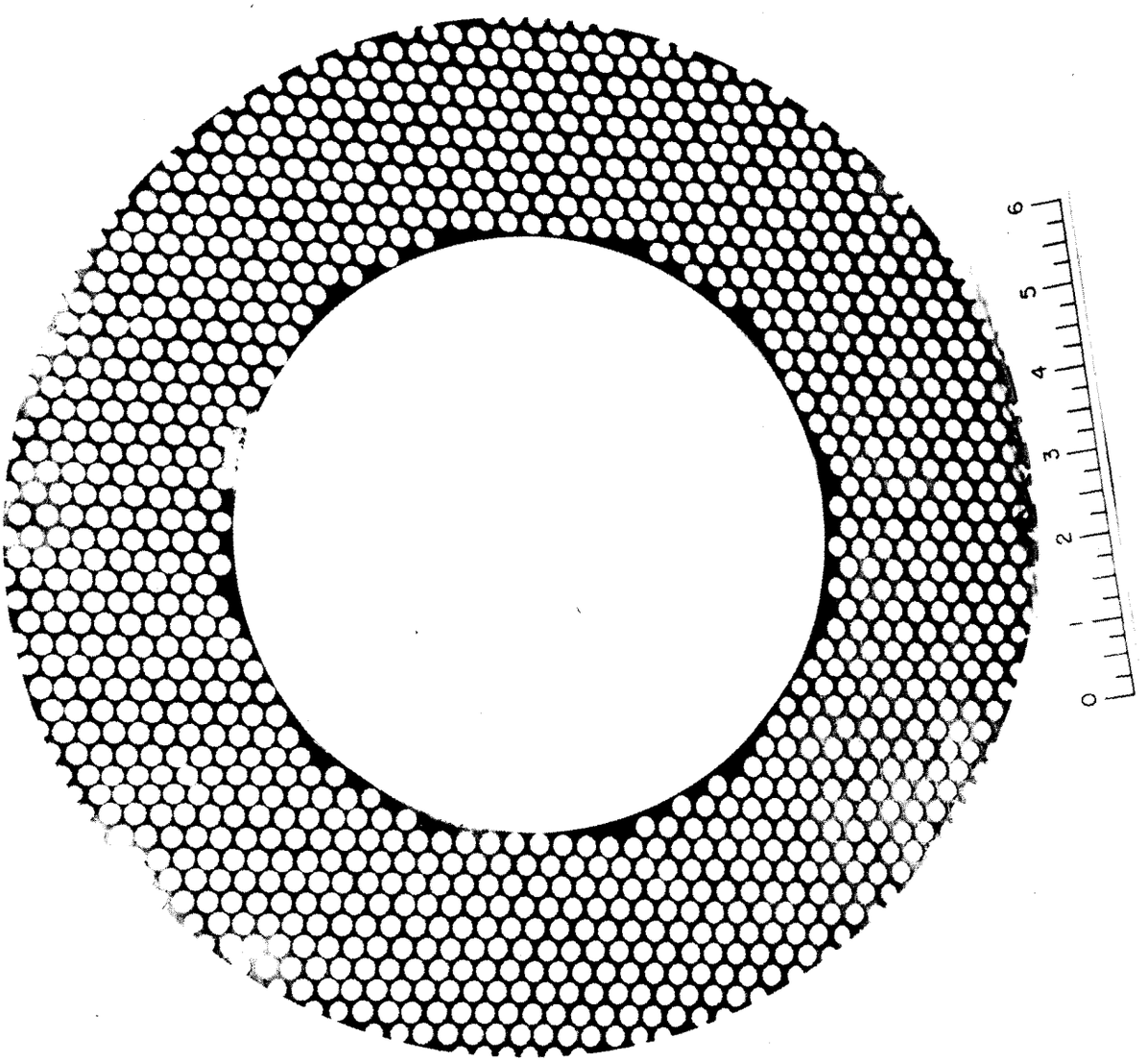

Figure 8 PUNCHED PLATE B, 70% OPEN AREA

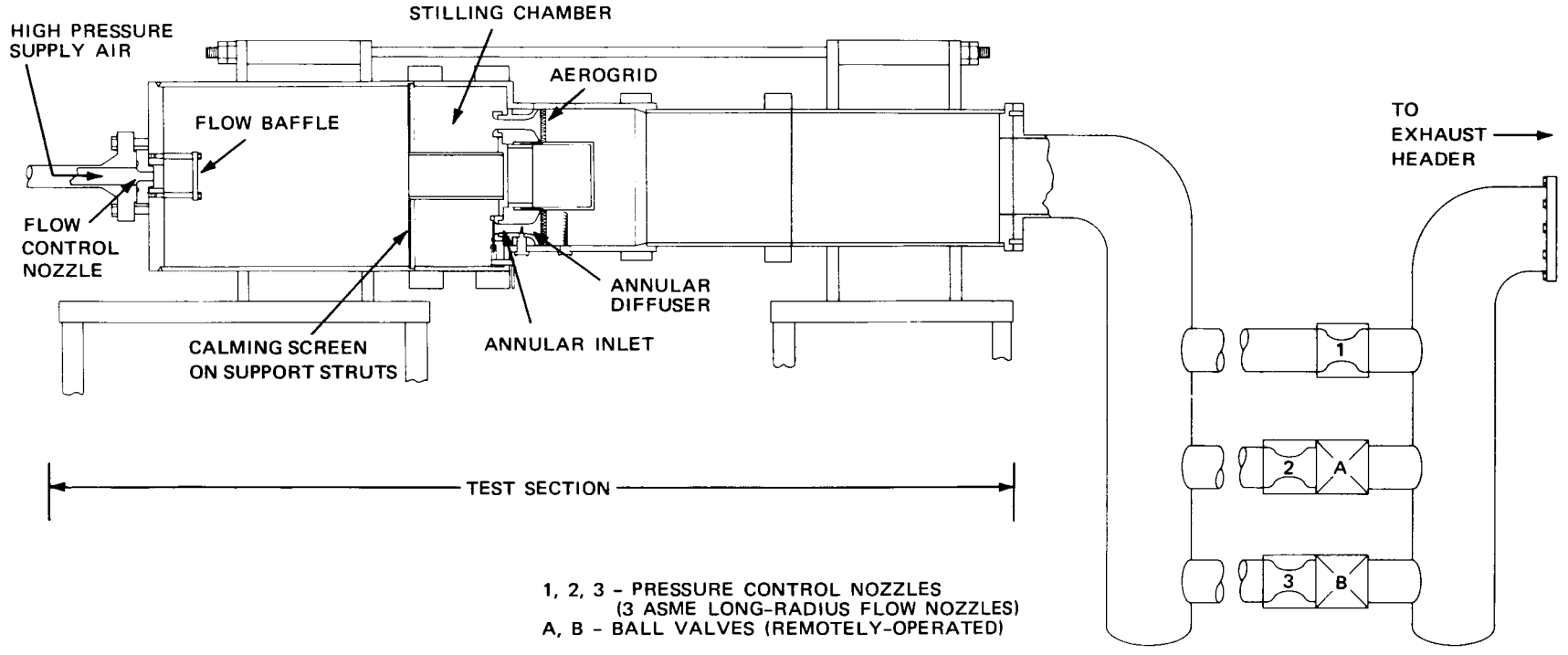

Figure 9 OVERALL FLOW SYSTEM

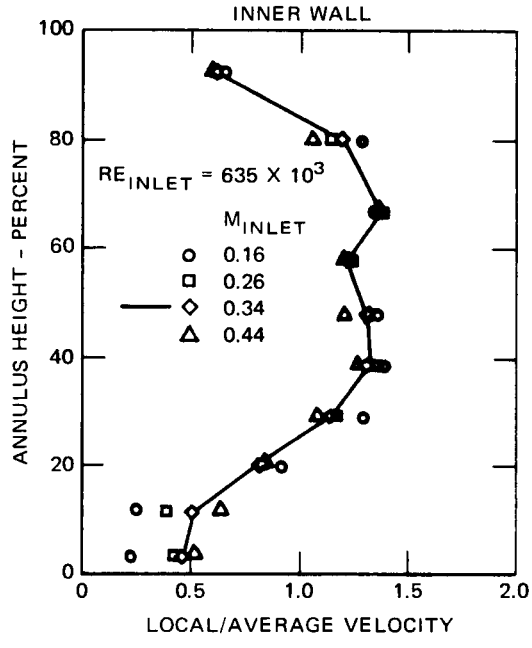

Figure 10 COMPARISON OF EXIT VELOCITY PROFILES FOR AEROGRID B AS A FUNCTION OF INLET MACH NUMBER

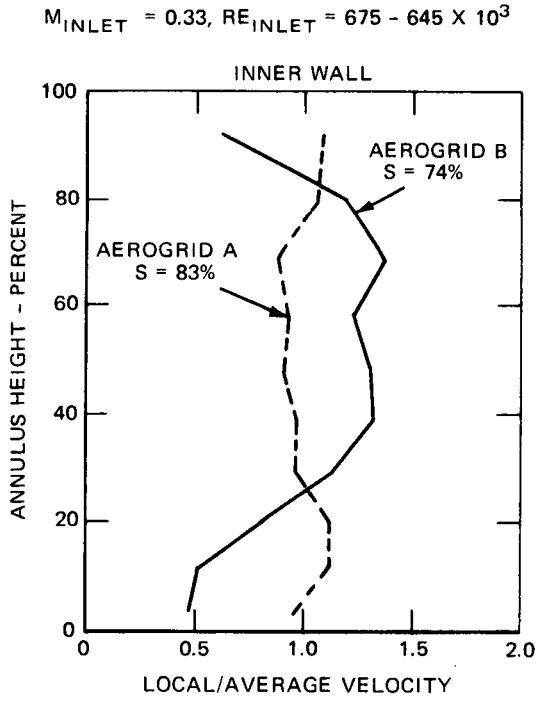

Figure 11 COMPARISON OF EXIT VELOCITY PROFILES FOR AEROGRIDS A AND B IN THE 0.1 IN. (0.254 cm) POSITION

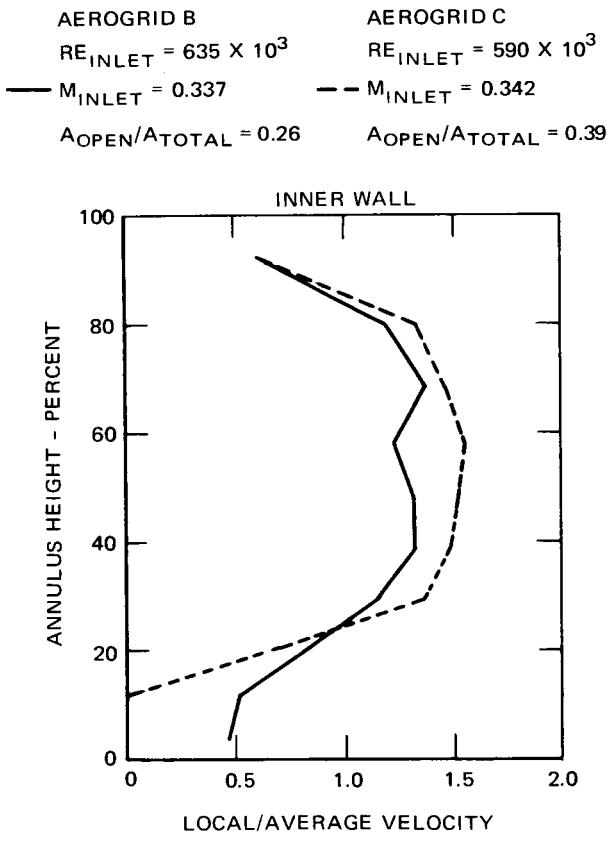

Figure 12 COMPARISON OF EXIT VELOCITY PROFILES FOR AEROGRIDS B AND C BOTH IN THE 0.1 IN. (0.254 cm) POSITION

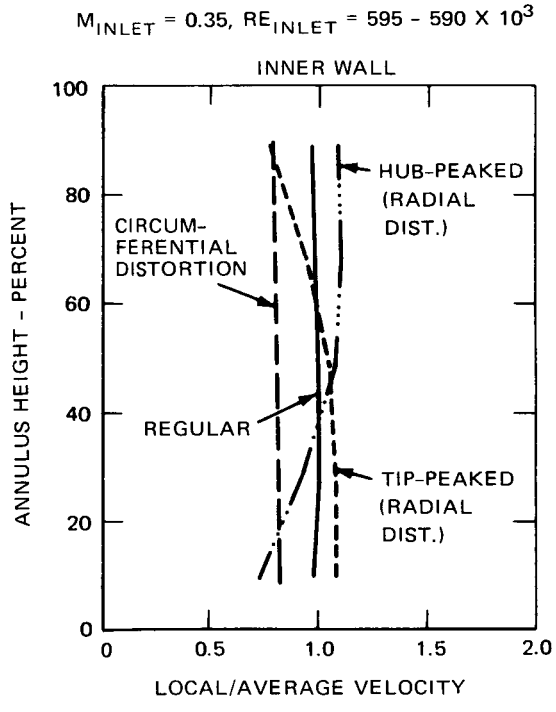

Figure 13 COMPARISON OF INLET VELOCITY PROFILES WITH TIP-PEAKED, HUB-PEAKED, REGULAR AND CIRCUMFERENTIAL DISTORTION FLOWS

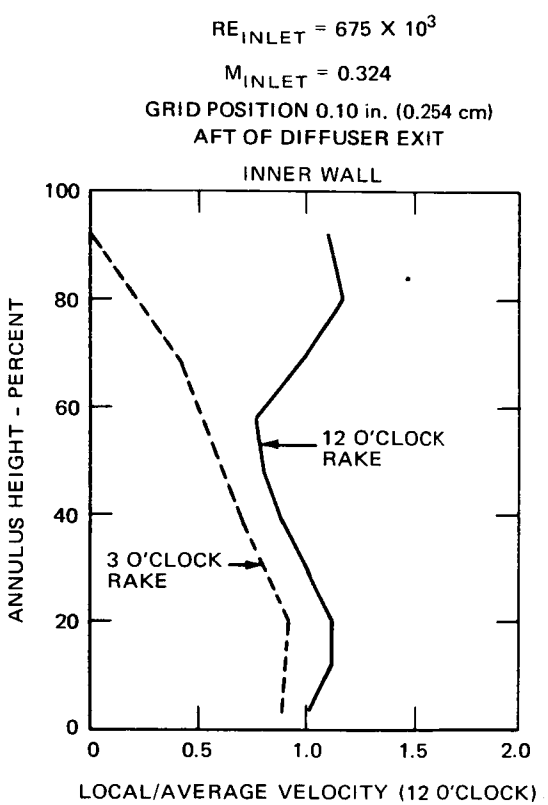

Figure 14 CIRCUMFERENTIAL VARIATION IN THE RADIAL VELOCITY PROFILE FOR AEROGRID A WITH RADIAL BLOCKAGE AT 3 O'CLOCK

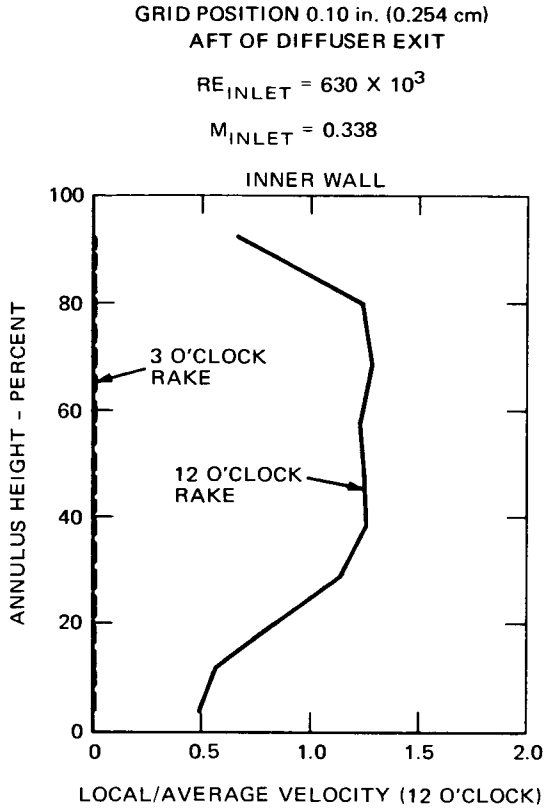

Figure 15 CIRCUMFERENTIAL VARIATION IN THE RADIAL VELOCITY PROFILE FOR AEROGRID B WITH RADIAL BLOCKAGE AT 3 O'CLOCK

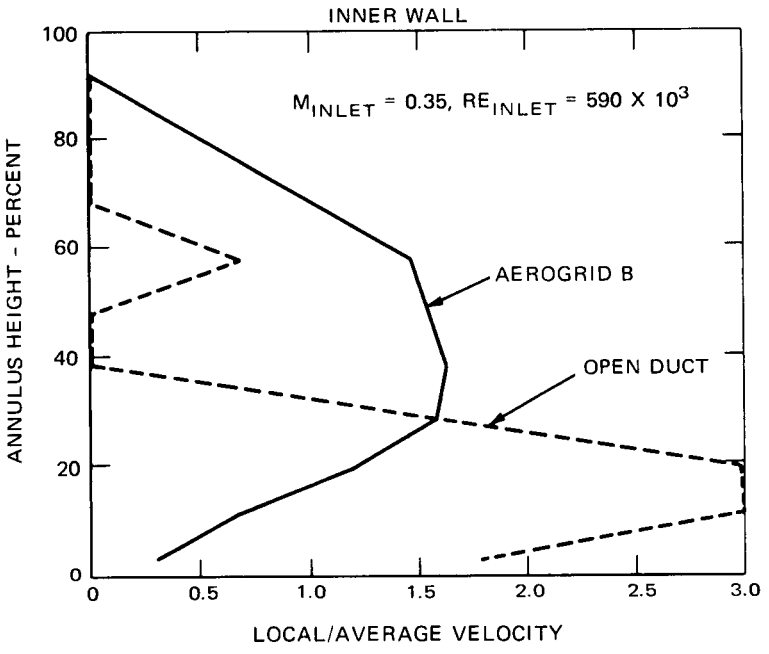

Figure 16 COMPARISON OF EXIT VELOCITY PROFILES WITH A TIP-PEAKED INLET FLOW PROFILE FOR THE DIFFUSER ALONE AND AEROGRID B IN THE FORWARD POSITION

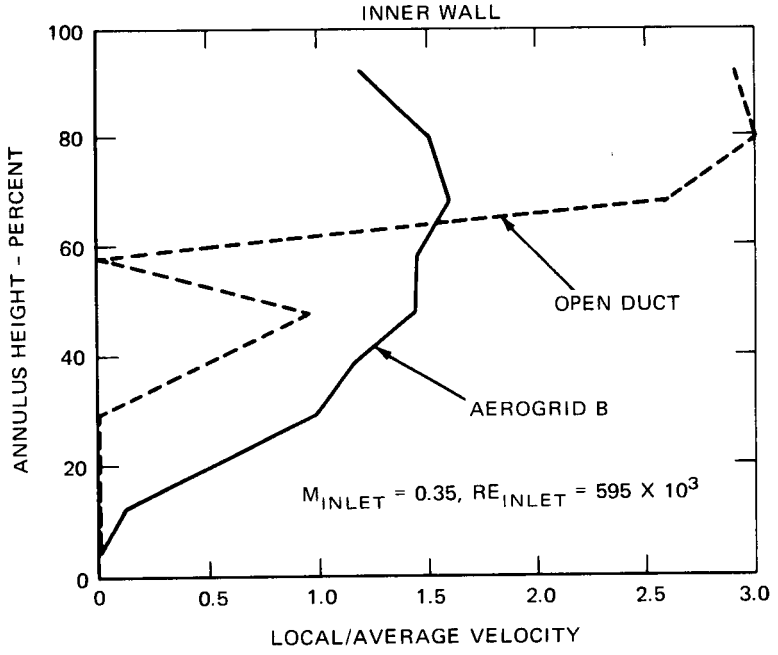

Figure 17 COMPARISON OF EXIT VELOCITY PROFILES WITH A HUB-PEAKED INLET FLOW PROFILE FOR THE DIFFUSER ALONE AND AEROGRID B IN THE FORWARD POSITION

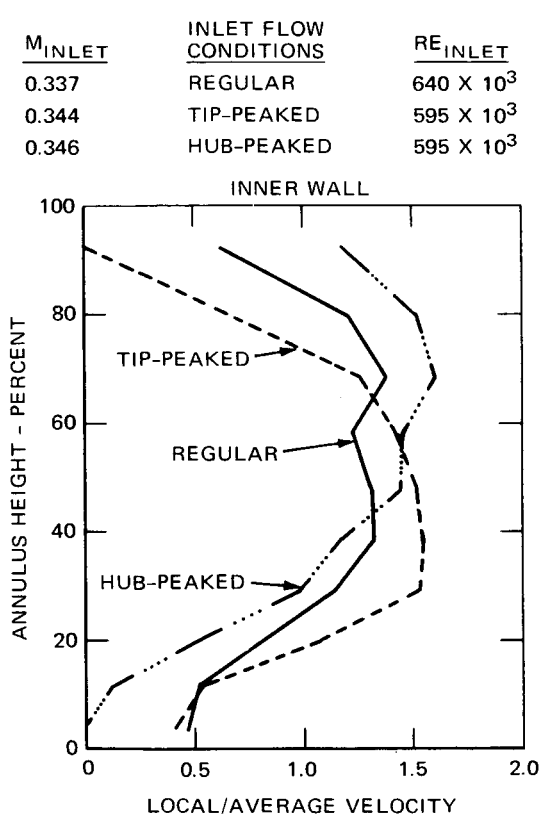

Figure 18 COMPARISON OF EXIT VELOCITY PROFILES FOR AEROGRID B IN THE FORWARD POSITION – REGULAR, TIP- AND HUB-PEAKED INLET FLOW

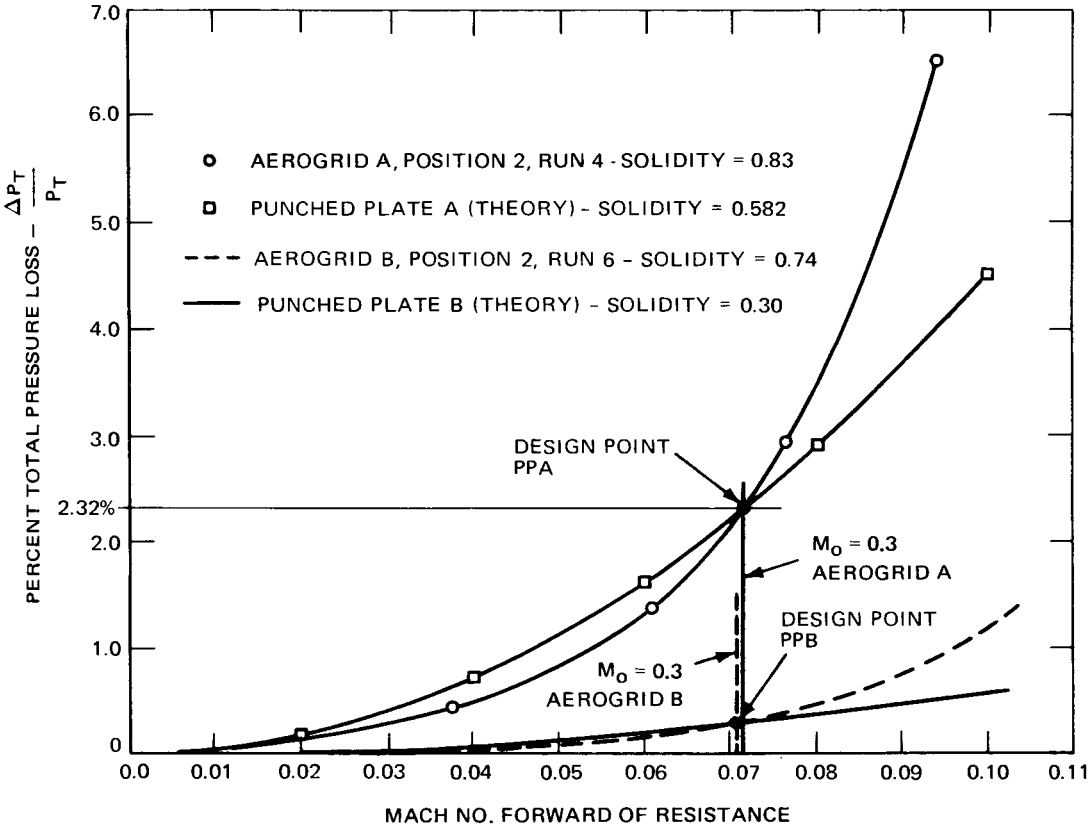

Figure 19 LOSS THROUGH A RESISTANCE, AEROGRID A AND PUNCHED PLATE A

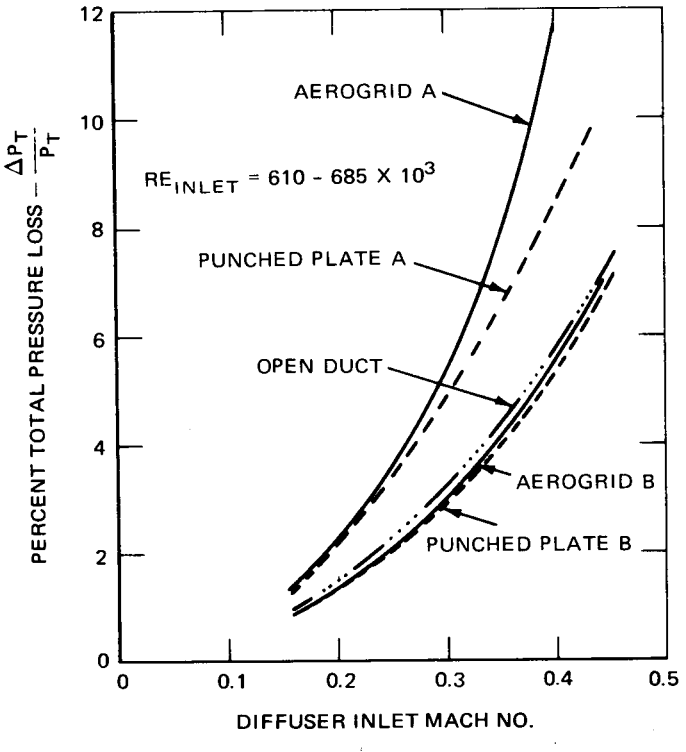

Figure 20 COMPARISON OF OVERALL TOTAL PRESSURE LOSS BETWEEN THE DIFFUSER ALONE, AEROGRIDS A AND B, PUNCHED PLATES A AND B IN THE 0.1 IN. (0.254 cm) POSITION

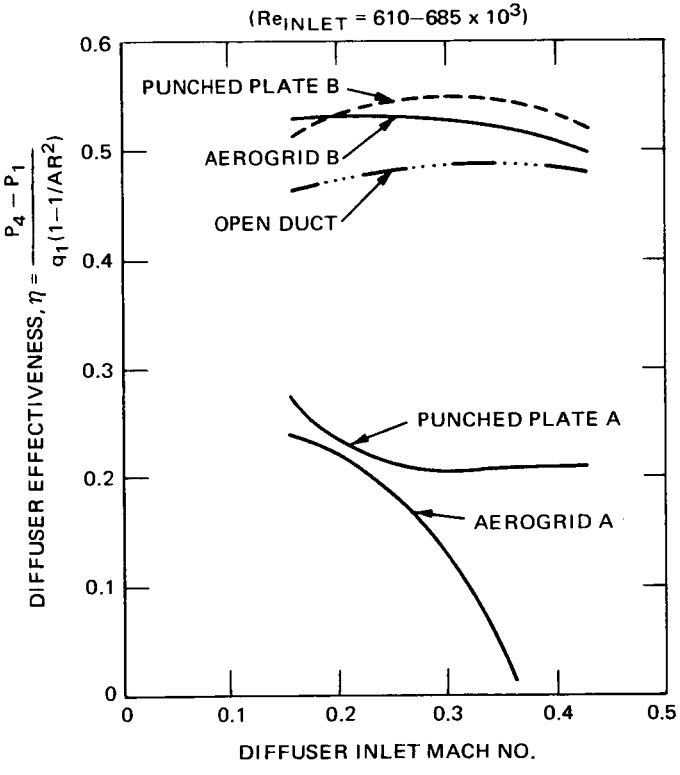

Figure 21 COMPARISON OF DIFFUSER EFFECTIVENESS BETWEEN THE DIFFUSER ALONE, AEROGRIDS AND A AND B, AND PUNCHED PLATES A AND B IN THE 0.1 IN. (0.254 cm) POSITION

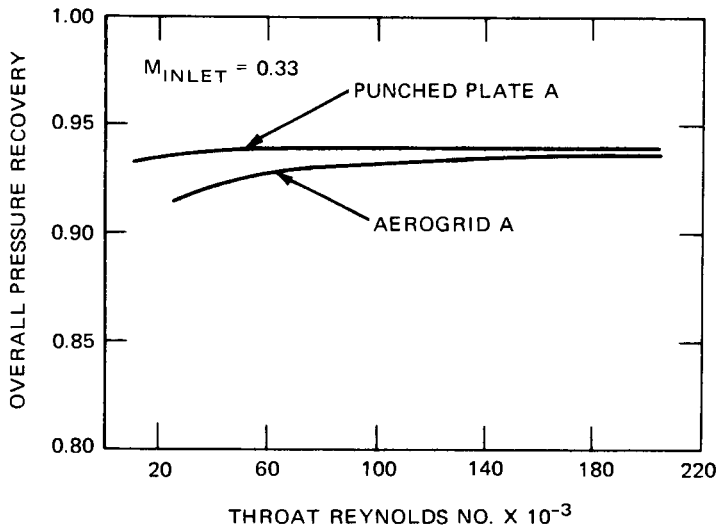

Figure 22 COMPARISON OF PRESSURE RECOVERY FOR AEROGRID A AND PUNCHED PLATE A IN THE FORWARD POSITION AS A FUNCTION OF THROAT REYNOLDS NUMBER

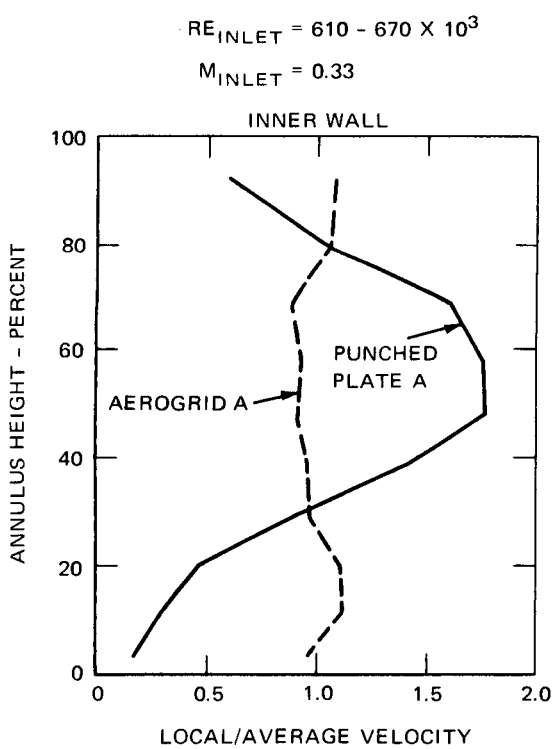

Figure 23 COMPARISON OF EXIT VELOCITY PROFILES FOR AEROGRID A AND PUNCHED PLATE A IN THE 0.1 IN. (0.254 cm) POSITION

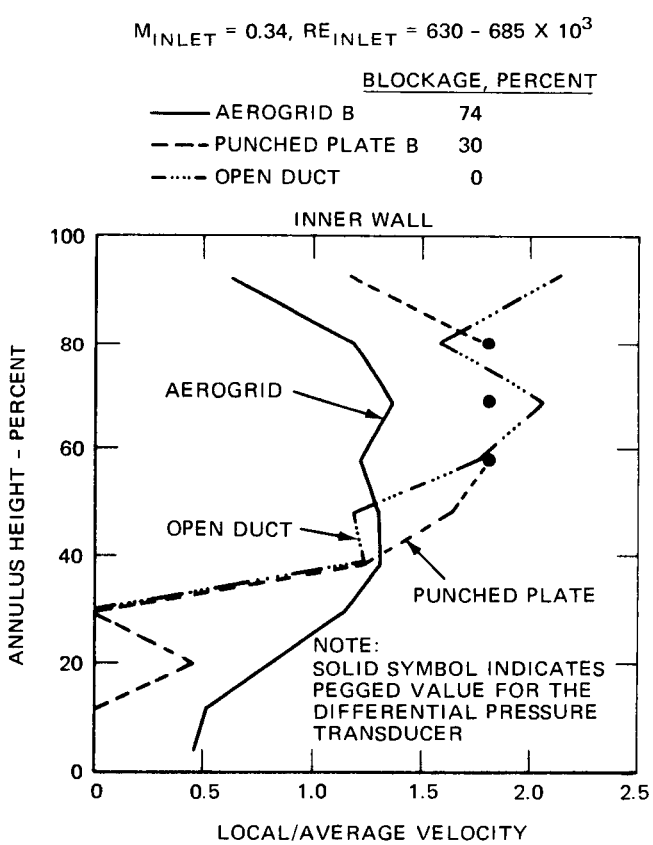

Figure 24 COMPARISON OF EXIT VELOCITY PROFILES FOR AEROGRID B, PUNCHED PLATE B, AND THE DIFFUSER ALONE

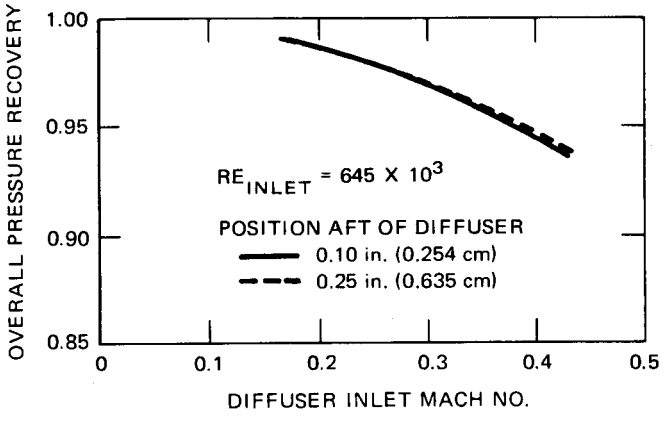

Figure 25a OVERALL PRESSURE RECOVERY WITH AEROGRID B IN TWO POSITIONS AS A FUNCTION OF INLET MACH NUMBER

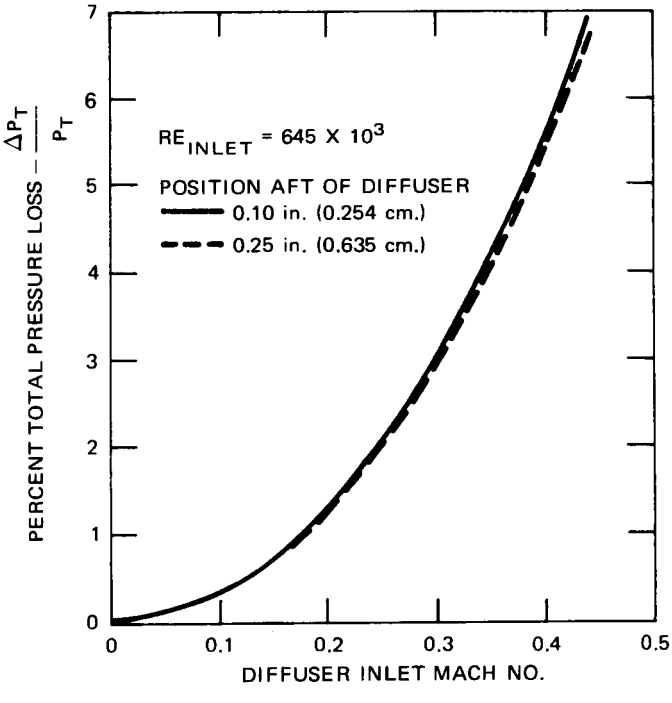

Figure 25b PERCENT OVERALL TOTAL PRESSURE LOSS WITH AEROGRID B IN TWO POSITIONS AS A FUNCTION OF INLET MACH NUMBER

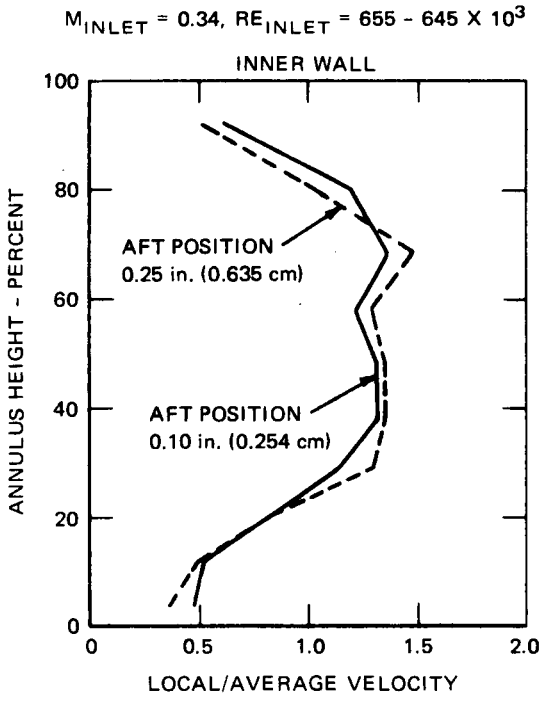

Figure 26 COMPARISON OF EXIT VELOCITY PROFILES FOR AEROGRID B IN THE 0.10 in. (0.254 cm) AND 0.25 in. (0.635 cm) POSITIONS AFT OF THE DIFFUSER EXIT PLANE

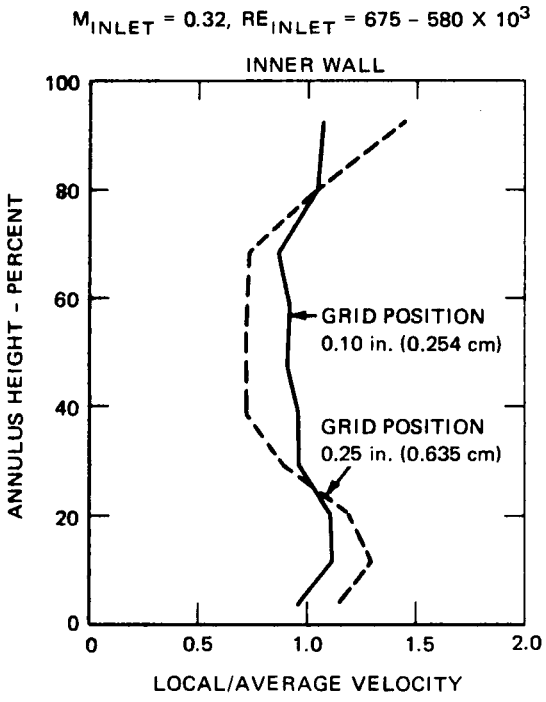

Figure 27 COMPARISON OF EXIT VELOCITY PROFILES FOR AEROGRID A AS A FUNCTION OF GRID POSITION AFT OF THE DIFFUSER EXIT

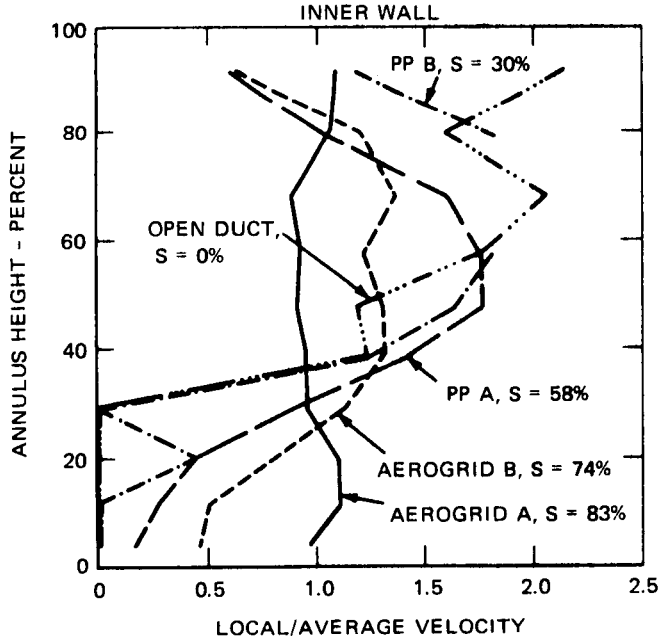

M_{INLET} = 0.34

ALL RESISTANCES WERE POSITIONED 0.10 in. (0.254 cm) AFT OF THE DIFFUSER EXIT PLANE

Figure 28 COMPARISON OF EXIT VELOCITY PROFILES FOR FLOW SMOOTHING AS A FUNCTION OF RESISTANCE SOLIDITY FOR AEROGRIDS A AND B AND PUNCHED PLATES A AND B REFERENCED TO THE DIFFUSER ALONE

THE JOHNS HOPKINS UNIVERSITY
APPLIED PHYSICS LABORATORY
SILVER SPRING, MARYLAND

DISTRIBUTION

NASA-Lewis Research Center
21000 Brookpark Road
Cleveland, Ohio 44135

Attention:	Report Control Office	MS 5-5	1
	Technology Utilization	3-19	1
	Library	60-3	2
	Fluid Systems Components Division	5-3	1
	W. L. Stewart	77-2	1
	L. Schopen	500-206	1
	J. B. Esgar	60-4	1
	W. T. Olson	3-16	1
	R. A. Rudey	60-6	1
	J. F. Dugan, Jr.	86-1	1
	Seymour Lieblein	501-5	1
	R. E. Jones	60-6	1
	Jack Grobman	60-6	1
	Lt. Col. G.S. Weden	500-317	1
	J. A. Albers	501-2	1
	A. J. Juhasz	60-4	25

S. C. Fiorello
Aeronautical Engine Laboratory
Naval Air Engineering Center
Philadelphia, Pennsylvania 1

Aerospace Research Laboratory
Wright-Patterson AFB, Ohio 45433
Attention: Dr. R. G. Dunn 1

NASA Scientific and Technical Information Facility
P.O. Box 33
College Park, Maryland 20740
Attention: NASA Representative
RQT-2448 6

FAA Headquarters
800 Independence Avenue, S.W.
Washington, D.C. 20533
Attention: R.W. Pinnes SS-120 1
Library 1

NASA Headquarters
600 Independence Avenue, S.W.
Washington, D.C. 20546
Attention: N.F. Rekos (RAP) 1
W.H. Roudebush (RAA) 1

THE JOHNS HOPKINS UNIVERSITY
APPLIED PHYSICS LABORATORY
SILVER SPRING, MARYLAND

Distribution (2)

Department of the Army
U.S. Army Aviation Material Laboratory
Propulsion Division (SAUFE-PP)
Fort Eustis, Virginia 23604
Attention: J. White 1
E.T. Johnson 1

United Aircraft of Canada, Ltd.
P.O. Box
Lonquenil, Quebec, Canada
Attention: Miss Mary Cullen 1

Air Force Office of Scientific Research
1400 Wilson Boulevard
Arlington, Virginia 22209
Attention: SREP 1

Defense Documentation Center (DDC)
Cameron Station
5010 Duke Street
Alexandria, Virginia 22314 1

Department of the Navy
Bureau of Naval Weapons
Washington, D.C. 20025
Attention: Robert Brown, RAPP14 1

Department of the Navy
Bureau of Ships
Washington, D.C. 20360
Attention: G.L. Graves 1

NASA-Langley Research Center
Langley Station
Technical Library
Hampton, Virginia 23365
Attention: M.R. Nichols 1
J.V. Becker 1
R.J. Margajon MS 404 1

United States Air Force
Aero Propulsion Laboratory
Area B, Bldg. 18D
Wright-Patterson A.F.B.
Dayton, Ohio 45433
Attention: R.E. Henderson 1

THE JOHNS HOPKINS UNIVERSITY
APPLIED PHYSICS LABORATORY
SILVER SPRING, MARYLAND

Distribution (3)

United Aircraft Corporation
Pratt & Whitney Aircraft Division
400 Main Street
East Hartford, Connecticut 06108

Attention:	G. Andreini		1
	Library		1
	R. Marshall		1

United Aircraft Research
East Hartford, Connecticut

Attention:	Library		1

Detroit Diesel Allison Division
Department 8894, Plant 8
P.O. Box 894
Indianapolis, Indiana 46206

Attention:	J.N. Barney		1
	G.E. Holbrook		1
	Library		1

Northern Research & Engineering Corp.
219 Vassar Street
Cambridge, Massachusetts 02139

Attention:	K. Ginwala		1

General Electric Company
Flight Propulsion Division
Cincinnati, Ohio 45215

Attention:	J.S. McBride	H-44	1
	F. Burggraf	H-32	1
	C. Danforth	H-32	1
	Technical Information Center	N-32	1
	D. Bahr		1

General Electric Company
1000 Western Avenue
West Lynn, Massachusetts 01905

Attention:	Dr. C.W. Smith		
	Library Building	2-40M	1

Curtiss-Wright Corporation
Wright Aeronautical Division
Woodridge, New Jersey 07075

Attention:	D. Wagner		1
	W. Walker		1

THE JOHNS HOPKINS UNIVERSITY
APPLIED PHYSICS LABORATORY
SILVER SPRING, MARYLAND

Distribution (4)

Air Research Manufacturing Company
402 South 36th Street
Phoenix, Arizona 85034
Attention: R.O. Bullock 1

Air Research Manufacturing Company
9851 Sepulveda Boulevard
Los Angeles, California 90009
Attention: L.C. Wright 1

AVCO Corporation
Lycoming Division
550 South Main Street
Stratford, Connecticut
Attention: C.W. Bolton 1
Charles Kuintzle 1

Continental Aviation & Engineering Corporation
12700 Kercheval
Detroit, Michigan 48215
Attention: E.H. Bernstein 1
H.C. Walch 1

International Harvester Company
Solar Division
2200 Pacific Highway
San Diego, California 92112
Attention: P.A. Pitt 1

Goodyear Atomic Corporation
Box 628
Piketon, Ohio
Attention: C.O. Langebrake 1

George Derderian - AIR 53662B
Naval Air Systems Command
Department of the Navy
Arlington, Virginia 20360 1

The Boeing Company
Commercial Airplane Division
P.O. Box 3991
Seattle, Washington 98124
Attention: G.J. Schott MS 80-66 1

THE JOHNS HOPKINS UNIVERSITY
APPLIED PHYSICS LABORATORY
SILVER SPRING, MARYLAND

Distribution (5)

The Boeing Company
Missile and Information Systems Division
224 N. Wilkinson Street
Dayton, Ohio 45402
Attention: W.K. Thorson 1

Aerojet-General Corporation
P.O. Box 1947
Sacramento, California 95809
Attention: M.S. Nylin 1
Library 1

Cornell Aeronautical Laboratory
4455 Genessee Street
Buffalo, New York 14221 1

Marquardt Corporation
16555 Saticoy Street
Van Nuys, California 91404 1

Thompson Ramo Wooldridge
23555 Euclid Avenue
Cleveland, Ohio 1

Aro, Incorporated
Arnold Air Force Station
Tennessee

Prof. J. M. Beer
Dept. of Chem. Eng. & Fuel Tech.
University of Sheffield
Mappin Street - Sheffield S1 3JD - Yorkshire
Great Britain 1

Cummings Engine Company
Cummings Technical Center
1900 McKinely Avenue
Columbus, Indiana 47201
Attention: Curt Dasbach MC 50142 1

Garrett/AiResearch Company
402 South 36th Street
Phoenix, Arizona 85034
Attention: J.M. Haasis 1

THE JOHNS HOPKINS UNIVERSITY
APPLIED PHYSICS LABORATORY
SILVER SPRING, MARYLAND

Distribution (6)

Pratt & Whitney Aircraft
Florida Research & Development Center
Box 2691
West Palm Beach, Florida 33402
Attention: J. Chamberlain 1
J. Dykslag 1
J. Shadowen 1
G. Lewis 1

Professor A. H. Lefebre
The Cranfield Institute of Technology
Cranfield, Bedford
Great Britain 1

Aerojet General Corporation
Sacramento Facility
P.O. Box 15847
Sacramento, California 95813
Attention: C.E. Tedmon 1
Dave Kors 1

The University of Toledo
Toledo, Ohio 43606
Attention: Dr. Duen-Ten Jeng 1
Dr. Kenneth DeWitt 1

Eaton Yale and Towne Research Center
26201 Northwestern Highway
Southfield, Michigan 48075 1

Rocketdyne
North American Rockwell
6630 Canoga Avenue
Canoga Park, California 91304
Attention: S.D. Clapp
Manager, Propulsion Technology Research Division 1

Department of Mechanical Engineering
201 Engineering Building
Michigan State University
E. Lansing, Michigan 48823
Attention: Dr. M.C. Potter 2

Clemson University
Clemson, South Carolina
Attention: Dr. Tah-teh Yang
Cook Engineering Bldg. 1

THE JOHNS HOPKINS UNIVERSITY
APPLIED PHYSICS LABORATORY
SILVER SPRING, MARYLAND

Distribution (7)

John W. Murrin - ORD 0331
Naval Ordnance Systems Command
Department of the Navy
Arlington, Virginia 20360 1

John A. Belding - AIR 330F
Naval Air Systems Command
Department of the Navy
Arlington, Virginia 20360

McDonnell-Douglas Company
Lambert-St. Louis Municipal Airport
P.O. Box 516
St. Louis, Missouri 63166
Attention: F.D. McVey 1

Ling-Temco Vought
Missiles & Space Division
P.O. Box 6267
Dallas, Texas 75222
Attention: R.O. Guthrie 1